

Supporting Information

Electron Transfer Dynamics and Excited state Branching in a Charge-Transfer Platinum(II) Donor-Bridge-Acceptor Assembly

Paul A. Scattergood,^{1#} Milan Delor,^{1#} Igor V. Sazanovich,^{1,2} Oleg V. Bouganov,³ Sergei A. Tikhomirov,³ Alexander S. Stasheuski,³ Anthony W. Parker,² Gregory M. Greetham,² Michael Towrie,² E. Stephen Davies,⁴ Anthony J. H. M. Meijer,^{1*} and Julia A. Weinstein^{1*}

¹ Department of Chemistry, University of Sheffield, Sheffield, S3 7HF, U. K.

² Central Laser Facility, Research Complex at Harwell, Rutherford Appleton Laboratory, Research Complex in Harwell, Harwell Science and Innovation Campus, Chilton, Oxfordshire, OX11 0QX, U. K.

³ B.I. Stepanov Institute of Physics, 68 Nezavisimosti Ave., Minsk, 220072, Belarus

⁴ School of Chemistry, The University of Nottingham, Nottingham NG7 2RD, U. K.

#The authors contributed equally to this work.

Synthesis - General Information

All starting materials were obtained from commercial suppliers and used as received. All solvents were of standard laboratory grade and were used without further purification. Dry solvents were obtained from a Grubbs solvent purification system and stored under argon. 'Degassing' of solvents was achieved through vigorous bubbling of argon for a period of at least 15 minutes. All synthetic manipulations were carried out using standard Schlenk line techniques under an atmosphere of argon. All intermediates and products were found to be stable to air and moisture and were stored in the dark at room temperature.

All ¹H NMR spectra were recorded on a 400 MHz BrukerAvance 400 spectrometer. ³¹P NMR spectra were obtained from Bruker DPX-400 and Avance 250 spectrometers with resonant frequencies for phosphorous nuclei of 162 and 101 MHz respectively. Deuterated solvents were purchased from Sigma-Aldrich and were of spectroscopic grade. All ¹H NMR spectra are calibrated with respect to the residual solvent peak (CHCl₃ 7.26) with chemical shifts being reported in ppm.

MALDI mass spectra were obtained from a Bruker Reflex III instrument using a time-of-flight (TOF) mass analyser. DCTB (*trans*-2-[3-(4-*tert*-butylphenyl)-2-methyl-2-propenylidene]malononitrile) was used as the matrix. Solid state mass spectra were obtained through use of an atmospheric solids analysis probe (ASAP, AP⁺). Electrospray Ionisation (ES⁺) mass spectra were collected via a Waters LCT TOF instrument. Electron Ionisation (EI⁺) mass spectra were obtained from a VG Autospec magnetic sector instrument.

4-bromo-*N*-octyl-1,8-naphthalimide

4-bromo-1,8-naphthalic anhydride (1.514 g, 5.46 mmol) and *n*-octylamine (3.75 ml, ρ = 0.78 g/ml, 22.63 mmol) were added to degassed ^{*i*}PrOH (50 ml) and refluxed for 24 hours. The resultant red-brown coloured solution was reduced in volume and cooled in ice for 15 minutes. MeOH (50 ml) was added to effect complete precipitation of the produced which was subsequently collected by filtration and washed with MeOH (4 x 50 ml) so that the filtrate showed no yellow colouration when spotted onto thin layer SiO₂. The pale yellow coloured solids were dried *in vacuo*. Yield = 0.983 g (2.53 mmol, 46%). ¹H NMR (CDCl₃): 0.86 (t, *J* = 7.04 Hz, 3H), 1.20-1.45 (m, 10H), 1.67-1.77 (m, 2H), 4.15 (t, *J* = 7.60 Hz, 2H),

7.84 (t, $J = 7.92$ Hz, 1H), 8.03 (d, $J = 7.88$ Hz, 1H), 8.41 (d, $J = 7.84$ Hz, 1H), 8.56 (dd, $J = 1.04, 8.56$ Hz, 1H), 8.65 (dd, $J = 1.00, 7.28$ Hz, 1H). ES-MS: $m/z = 388$ (MH⁺, 100%). Anal. Calc. for C₂₀H₂₂NO₂Br (%): C 61.86, H 5.71, N 3.61. Found (%): C 61.28, H 5.40, N 3.52.

4-ethynyl-*N*-octyl-1,8-naphthalimide

4-bromo-*N*-octyl-1,8-naphthalimide (1.000 g, 2.57 mmol), Pd(PPh₃)₂Cl₂ (94 mg, 0.13 mmol, 5.2 mol%), CuI (51 mg, 0.26 mmol, 10.3 mol%) and PPh₃ (34 mg, 0.13 mmol, 5.0 mol%) were added to previously degassed Et₃N and stirred at room temperature for 5 minutes. Excess trimethylsilylacetylene (1.45 ml, $\rho = 0.695$ g/mol, 10.26 mmol) was added, upon which the reaction mixture rapidly changed colour from yellow to dark brown. The solution was heated to 75 °C for 2 days, allowed to cool to room temperature and then the volatiles removed by rotary evaporation. The crude residue was redissolved in ether and filtered through a short silica plug to yield a bright yellow coloured filtrate which was subsequently evaporated to dryness. Removal of the trimethylsilyl protecting group was affected by adding the solids to a suspension of K₂CO₃ (1.434 g, 10.37 mmol) in degassed 1:2 (v/v) MeOH:CH₂Cl₂ (50 ml) which was then stirred at room temperature for 16 hours. The reaction was quenched by the addition of H₂O (60 ml) and the organic solvents completely removed by evaporation. The crude product was extracted from the aqueous suspension with CH₂Cl₂ (2 x 100 ml), with the organic phase being then washed with H₂O (1 x 50 ml), dried over MgSO₄ and reduced in volume. The product was purified by column chromatography (SiO₂, CH₂Cl₂) to afford a yellow coloured solid. Yield = 0.673 g (2.02 mmol, 78%). ¹H NMR (CDCl₃): 0.86 (t, $J = 7.08$ Hz, 3H), 1.19-1.46 (m, 10H), 1.66-1.77 (m, 2H), 3.73 (s, 1H), 4.16 (t, $J = 7.60$ Hz, 2H), 7.82 (t, $J = 7.84$ Hz, 1H), 7.93 (d, $J = 7.56$ Hz, 1H), 8.53 (d, $J = 7.60$ Hz, 1H), 8.64 (m, 2H). ES-MS: $m/z = 334$ (MH⁺, 100 %). Anal. Calc. for C₂₂H₂₃NO₂ (%): C 79.25, H 6.95, N 4.20. Found (%): C 79.00, H 6.69, N 4.15.

N-(4-iodobenzyl)-phenothiazine^[1]

All manipulations were carried out strictly under an Argon atmosphere. Degassed ⁱPr₂NH (0.60 ml, $\rho = 0.718$ g/ml, 4.25 mmol) was added to dry, degassed THF (20 ml) and cooled in an ice bath to 0 °C. ⁿBuLi in hexanes (2.65 ml, 1.6 M, 4.24 mmol) was added slowly and the mixture stirred in ice for 1 hour. A solution of phenothiazine (0.762 g, 3.82 mmol) in dry, degassed THF (20 ml) was transferred to the reaction vessel via cannula. The resultant bright yellow solution was stirred in ice and then allowed to warm slowly to room temperature. 4-iodobenzylbromide (1.260 g, 4.24 mmol) in dry, degassed THF (20 ml) was added via cannula and the reaction mixture then stirred at room temperature for 10 days. Removal of the solvent gave an oily residue which was redissolved in CH₂Cl₂ (125 ml) and poured *immediately* and *quickly* into saturated aqueous NaCl solution (200 ml). The organic phase was extracted, washed with 1x125 ml saturated aqueous NaCl followed by 1x125 ml H₂O and dried over MgSO₄. Removal of the solvent gave a light brown solid which was purified by column chromatography (SiO₂, 1:10 CH₂Cl₂:Hexane) to yield the product first as a clear oil and then as a bright white solid after thorough drying. Yield = 1.082 g (2.60 mmol, 68 %). ¹H NMR (CDCl₃): 5.01 (s, 2H), 6.59 (dd, $J = 0.68, 8.08$ Hz, 2H), 6.87 (td, $J = 1.04, 7.48$ Hz, 2H), 6.98 (td, $J = 1.60, 7.72$ Hz, 2H), 7.08 (td, $J = 1.52, 7.56$ Hz, 4H), 7.64 (d, $J = 8.36$ Hz, 2H). EI-MS: $m/z = 415$ (M⁺, 36%), 198 (M⁺-CH₂PhI, 100%). Anal. Calc. for C₁₉H₁₄NIS (%): C 54.95, H 3.40, N 3.37. Found (%): C 54.27, H 3.14, N 3.27.

N-(4-trimethylsilyl-ethynylbenzyl)-phenothiazine^[1]

N-(4-iodobenzyl)-phenothiazine (1.001 g, 2.41 mmol), Pd(PPh₃)₂Cl₂ (90 mg, 0.12 mmol, 5.3 mol%), and CuI (53 mg, 0.27 mmol, 11.5 mol%) were dissolved in degassed benzene (40

ml). Trimethylsilylacetylene (1.35 ml, $\rho = 0.695$ g/ml, 9.57 mmol) was added and the solution stirred at room temperature for 5 minutes before the addition of Et_3N (3.5 ml). A rapid colour change from orange to dark brown was observed upon addition of the amine reagent. The reaction solution was stirred at room temperature for 4 days and the solvent then removed by rotary evaporation. Column chromatography (SiO_2 , 1:5 DCM:Hexane) afforded the product first as a clear oil which was subsequently dried *in vacuo* to leave a white powder. Yield = 0.886 g. (2.29 mmol, 95%). $^1\text{H NMR}$ (CDCl_3): 0.23 (s, 9H), 5.06 (s, 2H), 6.59 (dd, $J = 0.96$, 8.16 Hz, 2H), 6.86 (td, $J = 1.08$, 7.53 Hz, 2H), 6.96 (td, $J = 1.60$, 7.57 Hz, 2H), 7.09 (dd, $J = 1.56$, 7.54 Hz, 2H), 7.25 (d, $J = 7.44$ Hz, 2H), 7.42 (d, $J = 8.28$ Hz, 2H). ES-MS: $m/z = 385$ (M^+ , 100%).

***N*-(4-ethynylbenzyl)-phenothiazine**

The trimethylsilyl protecting group was removed by dissolving *N*-(4-trimethylsilyl-ethynylbenzyl)-phenothiazine (665 mg, 1.72 mmol) in degassed 1:1 (v/v) MeOH:THF (40 ml). K_2CO_3 (605 mg, 4.36 mmol) was added and the reaction mixture then stirred rapidly at room temperature for 16 hours. The reaction was quenched with H_2O (30 mL) before the organic solvents were removed by rotary evaporation. The resulting aqueous suspension was extracted with 3 x 70 ml CH_2Cl_2 , with the combined organic layers being dried over MgSO_4 and the solvent removed to afford a clear oil. The product was purified by column chromatography (SiO_2 , 1:9 CH_2Cl_2 :Hexane) to give the pure product first as a clear oil and then as a white solid after thorough drying. Yield = 296 mg. (0.94 mmol, 55 %). $^1\text{H NMR}$ (CDCl_3): 3.05 (s, 1H), 5.07 (s, 2H), 6.59 (dd, $J = 1.00$, 8.12 Hz, 2H), 6.87 (td, $J = 1.12$, 7.48 Hz, 2H), 6.97 (td, $J = 1.60$, 7.52 Hz, 2H), 7.09 (dd, $J = 1.56$, 7.52 Hz, 2H), 7.27 (d, $J = 8.36$ Hz, 2H), 7.45 (d, $J = 8.24$ Hz, 2H). ES-MS: $m/z = 314$ (MH^+ , 100%), 199 ($\text{MH}^+ - \text{CH}_2\text{PhCCH}$, 18%). Anal. Calc. for $\text{C}_{21}\text{H}_{15}\text{NS}$ (%): C 80.48, H 4.82, N 4.47. Found (%): C 80.43, H 4.57, N 4.37.

***cis*-Pt(P^nBu_3) $_2\text{Cl}_2$**

P^nBu_3 (0.51 ml, $\rho = 0.81$ g/ml, 2.04 mmol) was added to a suspension of PtCl_2 (307 mg, 1.15 mmol) in dry, degassed CH_2Cl_2 (20 ml) which was then stirred at room temperature for 50 hours. The reaction solution was filtered to remove unreacted solids and then evaporated to dryness to leave a waxy grey mass. Purification was affected by thoroughly washing the crude material with small portions of hexane (3 x 20 ml), before redissolving the solids in diethyl ether. The ethereal solution was filtered and then evaporated to yield the product as a bright white crystalline powder. Yield = 456 mg (0.68 mmol, 66%). $^1\text{H NMR}$ (CDCl_3): 0.84-1.04 (m, 18H), 1.34-1.66 (m, 24H), 1.74-2.18 (m, 12H). $^{31}\text{P NMR}$ (CDCl_3): 0.95 ($J_{\text{Pt-P}} = 3519$ Hz). AP-MS: $m/z = 670$ (M^+ , 95%), 635 ($\text{M}^+ - \text{Cl}$, 100 %), 599 ($\text{M}^+ - 2\text{Cl}$, 32%). Anal. Cald. for $\text{C}_{24}\text{H}_{54}\text{Cl}_2\text{P}_2\text{Pt}$ (%): C 42.98 H 8.12. Found (%): C 42.49 H 8.21.

Ultrafast transient absorption apparatus.

The studies were performed in the Ultrafast Spectroscopy Laboratory, Rutherford Appleton Laboratory, STFC, UK, ULTRA [4] facility. Two synchronized 10 kHz, 8 W, 40 fs and 2 ps titanium sapphire oscillator/regenerative amplifiers (Thales) pump a range of optical parametric amplifiers (TOPAS). The broadband supercontinuum probe pulse was generated using a ~ 2 μJ portion of the 40 fs Ti:Sapph beam focused into 2-mm thick calcium fluoride plate mounted in a mechanical raster system. No reference beam was used in these experiments as the shot-to-shot stability of the probe light was not the limiting factor in obtaining high signal-to-noise. After passing through the sample, the probe beam was

collimated and focused into a spectrograph (0.25 m f/4 DK240, Spectral Products). The probe light was detected on a shot-by-shot basis on a 512-element silicon array (Quantum Detectors, QD) which has 1-mm-high active area and 0.05-mm pitch and is cooled to a temperature of -20°C using a Peltier system. The 400 nm beam from the second harmonic of the Ti:Sapph laser was used for sample excitation. The probe and pump beam diameters in the sample were about 80 and 200 μm , for probe and pump respectively. The pump energy at the sample was 0.3 μJ and the relative polarisation was set to magic angle. Prior to experiments, the linearity of sample response was checked at the excitation energies used. All experiments were carried out in Harrick cells with 2 mm thick CaF_2 windows with 500 to 950 μm sample path length and a typical optical density of 0.5 to 1 at 400 nm. All samples were mounted on a 2D-raster stage and solutions were flowed to ensure photostability.

Electrochemistry

Cyclic voltammograms were recorded via an Autolab Potentiostat 100 using GPE Software. Analyte solutions were prepared using N_2 -saturated dry CH_2Cl_2 obtained from a Grubbs solvent purification column, having a typical concentration of 1.65 mmol dm^{-3} . All measurements were conducted at r. t. under a positive pressure of solvent saturated N_2 . $[\text{N}^n\text{Bu}_4][\text{PF}_6]$ was used as a supporting electrolyte, being recrystallised from ethanol and oven dried prior to use. The cell comprised a Pt disc working electrode, a Pt wire counter electrode and a Ag/AgCl reference electrode chemically isolated from the analyte solution by an electrolyte-containing bridge tube tipped with a porous frit. Ferrocene was used as an internal reference; all potentials are quoted relative to the Fc^+/Fc couple.

The UV-vis spectroelectrochemical experiments were accomplished using an optically transparent electrochemical (OTE) cell (in a modified quartz cuvette, optical path length: 0.5 mm).[2] A three-electrode configuration was employed; this consisted of a Pt/Rh gauze working electrode, a Pt-wire secondary electrode (in a fritted PTFE sleeve), and a saturated calomel electrode (SCE) that was chemically isolated from the test solution via a bridge tube containing electrolyte solution and terminated in a porous frit. The potential at the working electrode was controlled by a Sycopel Scientific DD10M potentiostat. UV-vis spectra were recorded on a Perkin Elmer Lambda 16 spectrophotometer; the cavity was purged with N_2 and the temperature of the sample (243 K) was controlled by flowing cooled N_2 across the cell surface. The FTIR spectroelectrochemical experiment were performed using Autolab PGSTAT100 potentiostat in an optically transparent thin-layer electrochemical cell that consisted of a modified solution cell (Specac) (optical pathlength ca. 200 μm) with CaF_2 windows and three-electrode configuration; Pt- minigrad working and secondary electrodes and a twinned Ag wire reference electrode.[3] IR spectra were recorded at ambient temperature on a N_2 -purged Perkin Elmer FTIR spectrometer.

Cyclic voltammograms for complexes 1-4 are shown in Fig. S1a, and for ligand precursors *N*-(4-ethynylbenzyl)-phenothiazine (*PTZ-H*) and *N*-(4-iodobenzyl)-phenothiazine (*PTZ-I*) - in figure S1b.

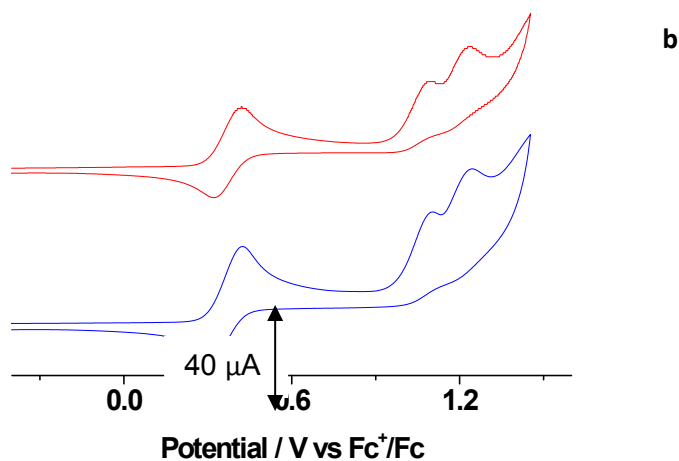
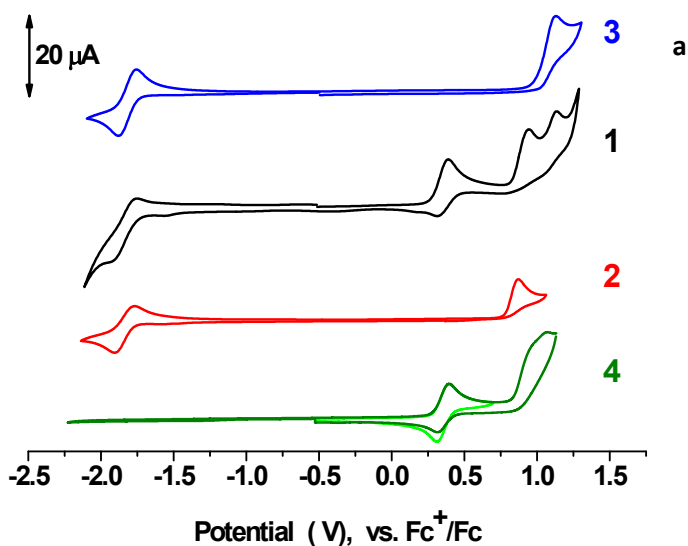


Figure S1. Cyclic voltammograms recorded at 100 mVs^{-1} for CH_2Cl_2 solutions with 0.2 M $[\text{NBu}_4][\text{PF}_6]$ as supporting electrolyte. The potentials are quoted against Fc^+/Fc .

a. CV of complexes **3** (blue), **1** (black), **2** (red), **4** (green; the isolated redox couple is shown in light green) at r.t. **b.** CV of *N*-(4-iodobenzyl)-phenothiazine (PTZ-I, top) and *N*-(4-ethynylbenzyl)-phenothiazine (PTZ-H, bottom).

Table S1. Electrochemical data for ‘PTZ-I’ and ‘PTZ-H’ measured in CH_2Cl_2 solutions containing 0.2 mol dm^{-3} $[\text{NBu}_4][\text{PF}_6]$. Values are quoted against the Fc^+/Fc couple in mV. For reversible couples, the peak separation is shown in brackets.

Compound	$E_{\frac{1}{2}\text{Ox}^1} (\Delta E_{a,c}) / \text{V}$	$E_{a,p}\text{Ox}^2 / \text{V}$	$E_{a,p}\text{Ox}^3 / \text{V}$
PTZ-I	+0.37 (0.10)	+1.09	+1.24
PTZ-H	+0.37 (0.11)	+1.10	+1.24

Emission spectroscopy

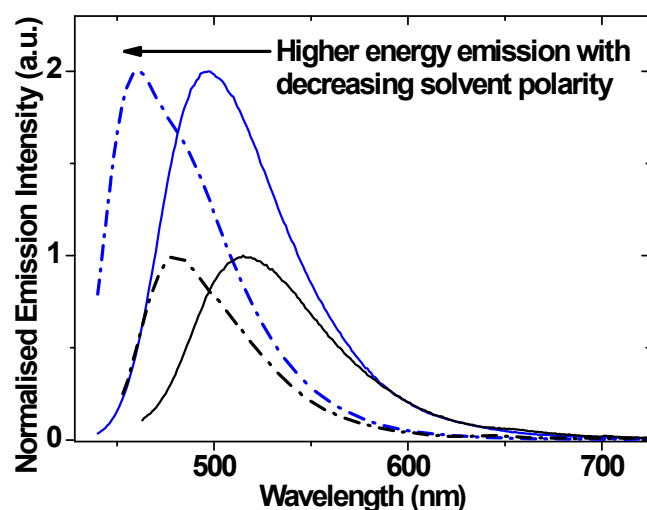


Figure S2. Emission profiles for **1** (black) and **3** (blue) in CH₂Cl₂ (solid lines) and the less polar Toluene (dot-dashed lines). The latter shows higher energy emission. This solvatochromism is characteristic for emission arising from charge transfer bands. It is worth noting that the emission in Toluene is more structured, with visible vibronic bands. In this figure the low energy emission observed in figure 4 of the main text is quenched by the presence of oxygen in the solution.

Nanosecond flash photolysis.

Nanosecond Flash Photolysis studies were conducted at the University of Sheffield, UK on a home-built setup using a tuneable Ti:Sapph laser. was pumped with the second harmonic (532 nm) of a Q-switched Nd:YAG laser LS-2137U (LOTIS TII) to obtain a second-harmonic pulse output centred at 420 nm (10 Hz repetition rate, 25 ns pulsewidth) with energy kept at about 2.0 mJ per pulse. The probe and pump beam diameters are approximately 2.5 and 4 mm, respectively. Probing was performed with a steady-state 150 W Hamamatsu Arc Xe lamp. The probe beam was detected by a monochromator equipped with a home-built detector unit, based on FEU-118 PMT. Detector current output was coupled into a Tektronix TDS 3032B digital oscilloscope and subsequently transferred to a computer.

The transient absorption spectra for a degassed solution of **1** in CH₂Cl₂ following laser excitation at 420 nm (≈ 25 ns pulse width) show a broad ground state bleach centred at 430 nm and the formation of a very broad transient with a maximum at 680 nm, which corresponds to that previously published for the triplet state of ethynyl-substituted NAP,^[12] confirming that ³NAP is the lowest excited state in **1**. Under optically dilute conditions ($OD_{430\text{nm}} \approx 0.05$ in 1 cm pathlength), the spectral decay is mono-exponential with lifetime $\tau \approx 190 \pm 10 \mu\text{s}$. At higher concentrations, the spectral decay becomes uniformly non-monoexponential, likely due to typical concentration effects associated with bi-molecular triplet-triplet annihilation. This effect was not explored further, and the concentrations were maintained below this effect. The ³NAP emission lifetime measured on the same laser setup under optically dilute conditions was found to also be $\sim 190 \pm 10 \mu\text{s}$ at r.t. for **1-3**.

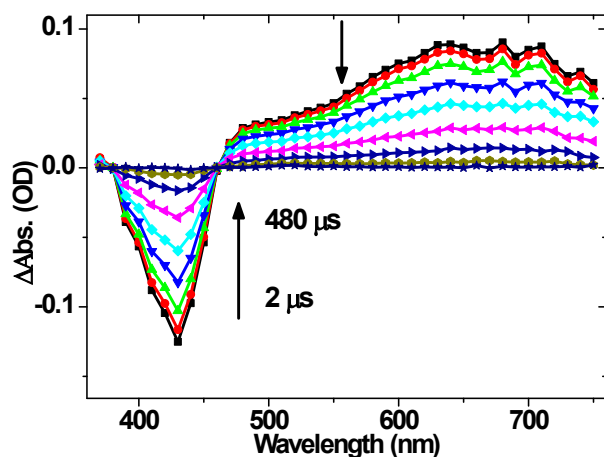


Figure S3. Transient absorption spectra of a degassed solution of **1** in CH_2Cl_2 at r.t. after 420 nm, ~ 25 ns excitation. The ground state bleach and transient bands decay synchronously.

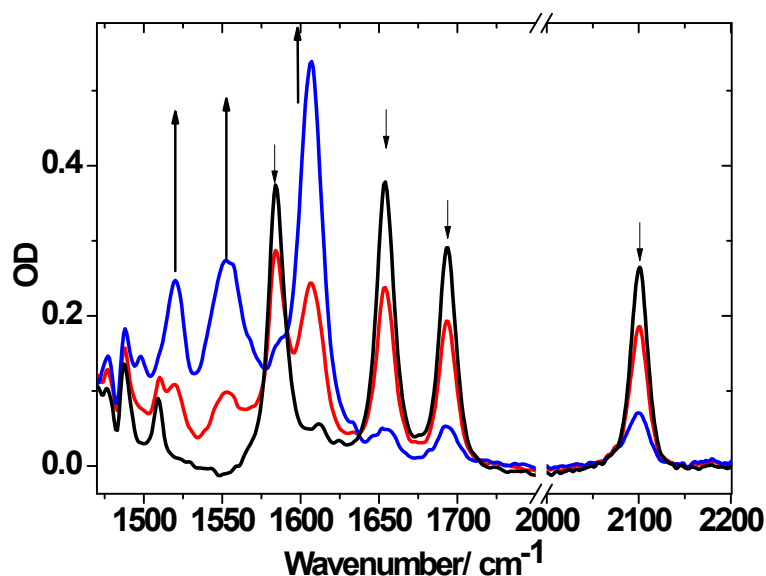


Figure S4. IR Spectroelectrochemistry of **3**. Spectral changes accompanying one-electron reduction of **3** at r.t., in CH_2Cl_2 in presence of 0.2M $[\text{Bu}_4\text{N}][\text{PF}_6]$, in the IR OTTLE cell. Black spectrum: neutral **3**; red spectrum: an intermediate point where both the neutral and the reduced forms are present; blue spectrum: almost totally reduced form, **3** \cdot^- .

Singlet oxygen quantum yields were measured on a home-built setup by comparative technique using perinaphthenone in CH_2Cl_2 as a standard.[5] The sample solutions were excited at 355 nm with the third harmonic of the pulsed Q-SW Nd:YAG laser (LS-1231M from LOTIS TII). The excitation radiation was focused onto the sample into $\text{Ø}4$ mm spot.

The time-resolved signal of $^1\text{O}_2$ luminescence at 1275 nm was detected with an InGaAs photodiode of $\text{Ø}3$ mm active area (J22D-M204-R03M-60-1.7, Judson Technologies, LN-cooled). The output from the photodiode was coupled into the low-noise current amplifier (DLPCA-200, FEMTO Messtechnik GmbH), the amplifier output signal was recorded with a digital oscilloscope (TDS 3032B Tektronix) and transferred to the computer. To selectively detect the $^1\text{O}_2$ emission, the high-contrast bandpass optical filter (1277 nm center wavelength, 28 nm FWHM, custom-made by Izovac, Belarus) was fitted in front of the InGaAs

photodiode. To increase the light collection efficiency, the spherical broadband mirror was set behind the sample to reflect the NIR emission through the sample towards the detector.

The optical densities of both the studied compound and the standard were matched at 355 nm, and the same solvent was used for both the studied compound and the standard. The series of experiments was performed at set of different excitation energies ranging from 55 μJ to 420 μJ per pulse. The presented $\phi(^3\text{O}_2)$ values were obtained in low-energy limit, for which the decay of singlet oxygen emission was mono-exponential.

Ultrafast Spectroscopy - further analysis

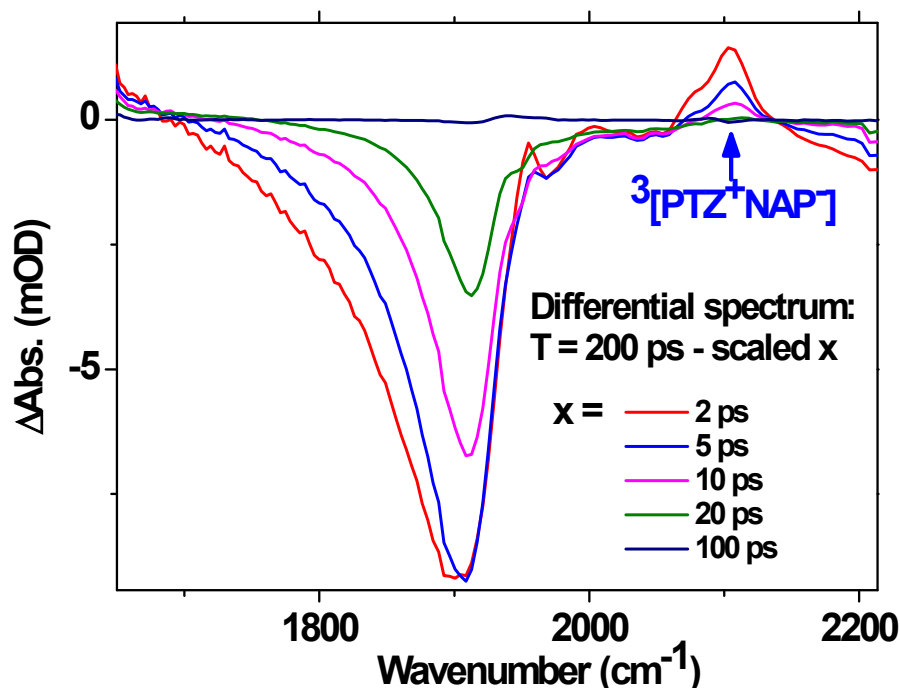


Figure S5. Evidence for the presence of an acetylide band for the 3 CSS state for **1** in CH_2Cl_2 at room temperature. TRIR differential spectra obtained by subtracting early-time spectra from $T = 200$ ps. Early-time spectra are scaled so that the ground-state bleaches cancel out, allowing to see the evolution of the 2105 cm^{-1} signal associated with $\nu(\text{C}\equiv\text{C})$ in the 3 CSS state. At $T = 200$ ps, the CT manifold has fully decayed into its product states. In other words, 3 CSS has already reached maximum population, and with a decay lifetime of 1 ns, little of it will have decayed by 200 ps. Therefore in this differential spectrum of $T = 200$ ps – x , an indication of population of 3 CSS is manifested by a *decrease* in associated band intensity. The state is fully populated when the band isn't visible anymore. This figure therefore shows that 3 CSS is almost fully populated by 20 ps.

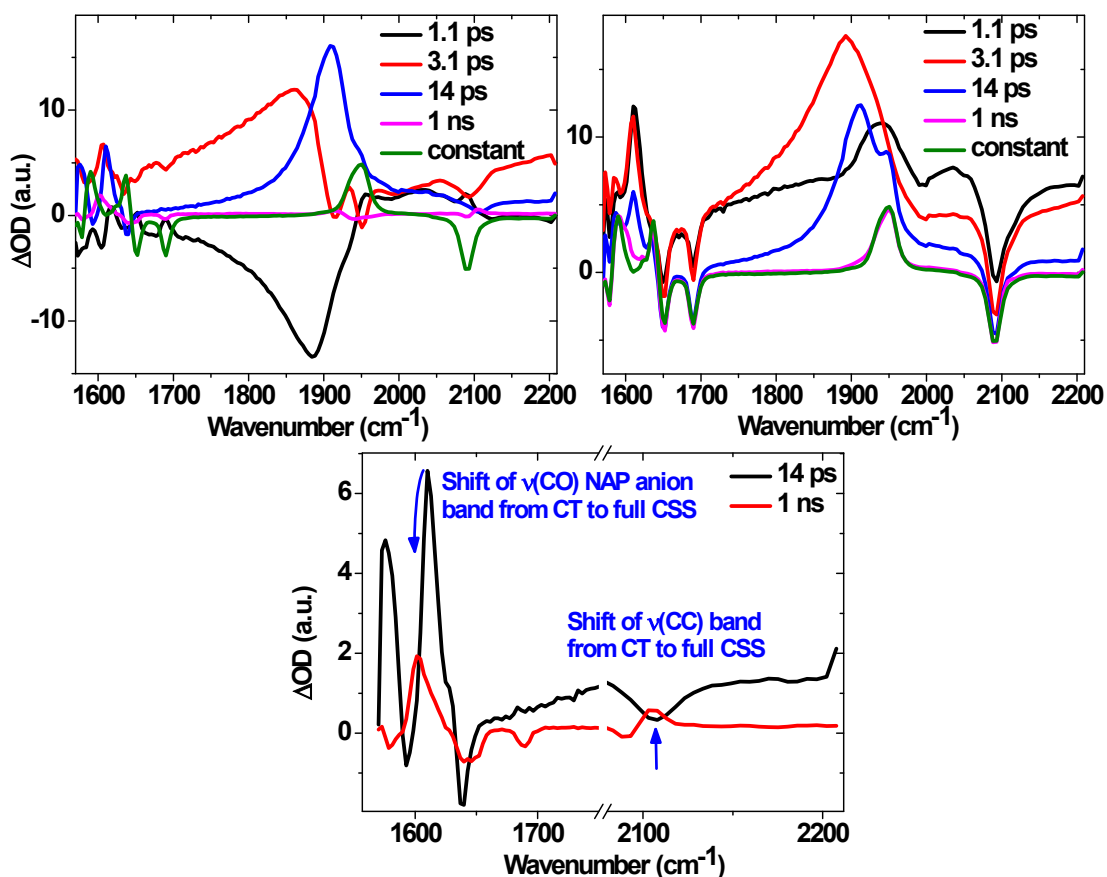


Figure S6. Decay Associated Spectra (DAS, top left), Evolution Associated Spectra (EAS, top right) and detail of the DAS (bottom) for the TRIR of **1** in CH_2Cl_2 , using a global sequential analysis. The DAS and EAS are extracted from the global analysis performed with open-source software Glotaran. The DAS reflect the spectral contribution of each globally fitted decay component, whilst the EAS show the resulting spectral evolution assuming a sequential model. The DAS allow identifying the species associated with each lifetime. From this analysis the shifts of the C=O and C=C bands are evident as the CT state decays into the full ^3CSS .

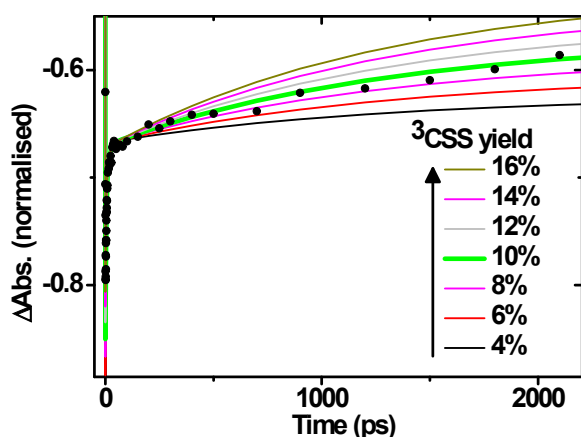


Figure S7. Same data as in figure 11b of the main text, but with all concentration profiles normalised at 28 ps – this is to show that the parameter that best constrains the yields of product states is the slope of the well-resolved 1 ns ^3CSS decay component.

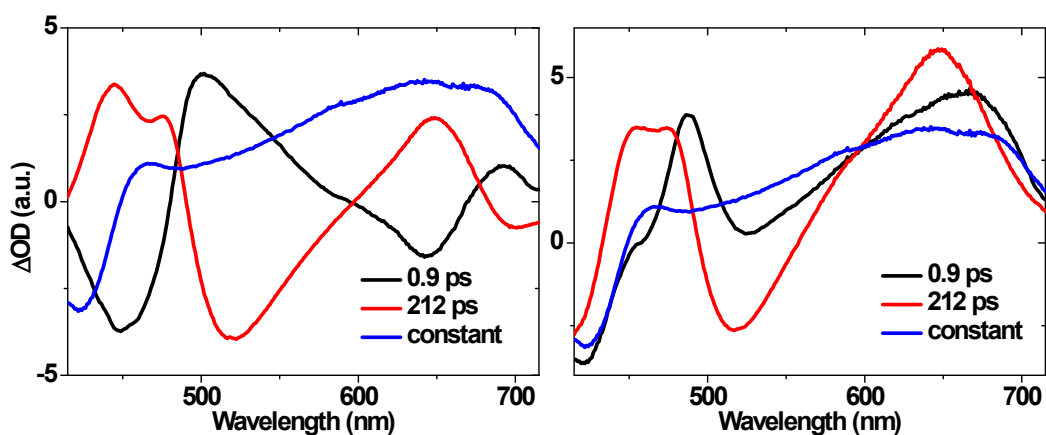


Figure S8. Decay Associated Spectra (DAS, left) and Evolution Associated Spectra (EAS, right) of the ultrafast TA following 400 nm excitation for **3** in CH_2Cl_2 . The DAS and EAS are extracted from the global analysis performed with open-source software Glotaran. The DAS reflect the spectral contribution of each globally fitted decay component, whilst the EAS show the resulting spectral evolution assuming a sequential model. The DAS allow identifying the species associated with each lifetime. The black line (DAS1) represents the first species that is picked up in these experiments, which has a 0.9 ps lifetime. The negative-going feature at 450 nm is tentatively assigned to stimulated emission from the initially populated MLCT manifold, which decays into a longer-lived, lower energy stimulated emission at around 520 nm (DAS2, red, see text for details on assignments). DAS1 and DAS2 have almost identical spectral profiles for all three complexes **1**, **2** and **3**, indicating that the nature of their initially populated excited states is similar.

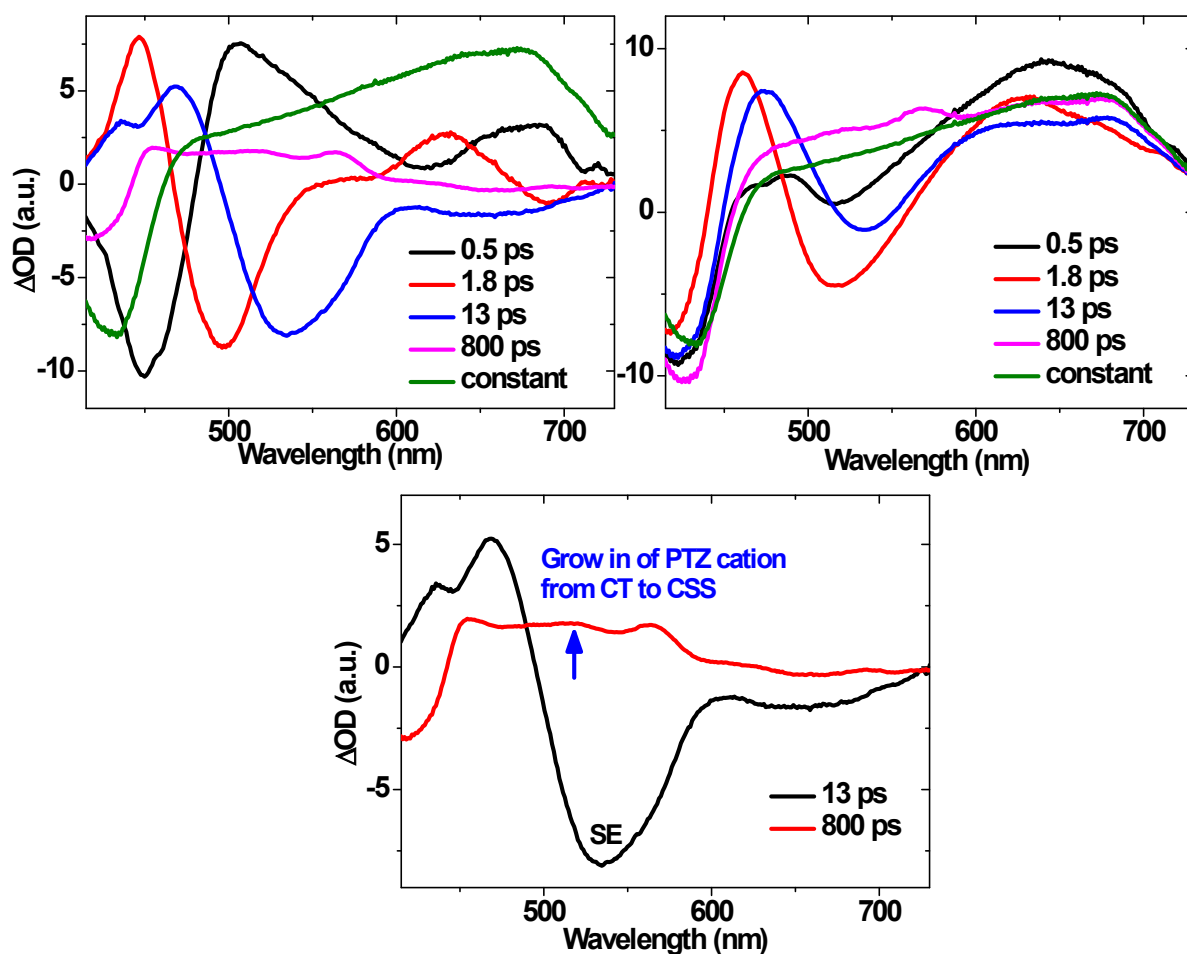


Figure S9. Decay Associated Spectra (DAS, top left), Evolution Associated Spectra (EAS, top right) and detail of the DAS (bottom) for the ultrafast TA of **1** in CH_2Cl_2 . The growth of the PTZ cation band as the full ^3CSS is formed is evident. DAS1 and DAS2 have similar spectral profiles for **1**, **2** and **3**. See text for details of assignments.

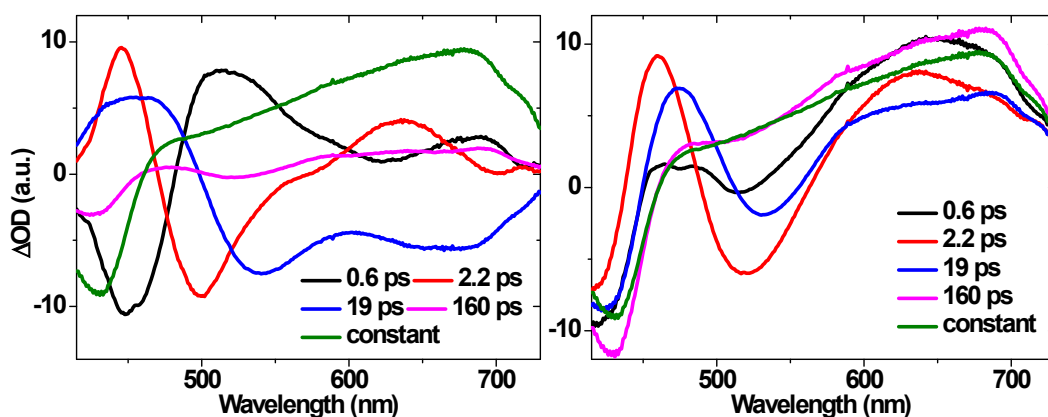


Figure S10. Decay Associated Spectra (DAS, left) and Evolution Associated Spectra (EAS, right) for the ultrafast TA of **2** in CH_2Cl_2 . DAS1 and DAS2 have similar spectral profiles for **1**, **2** and **3**. See text for details of assignments.

Solvent Polarity effect on excited state dynamics of 1. The presence of several close-lying excited states of different origin potentially allows tuning of their relative order and dynamics through changes in solvent polarity. Ultrafast spectroscopic studies of **1** in acetonitrile were therefore carried out (see figures S11a and S11b for TRIR and TA data) in order to explore how the dynamics of close-lying excited states can be influenced by solvent polarity. In this more polar solvent, the energy of the initial CT states and ^3CSS states are lower than that in CH_2Cl_2 , increasing the rate of their decay to the ground and ^3NAP states, decreasing the lifetimes to 6.3 ± 0.5 ps (CT) and 60 ± 10 ps (^3CSS).

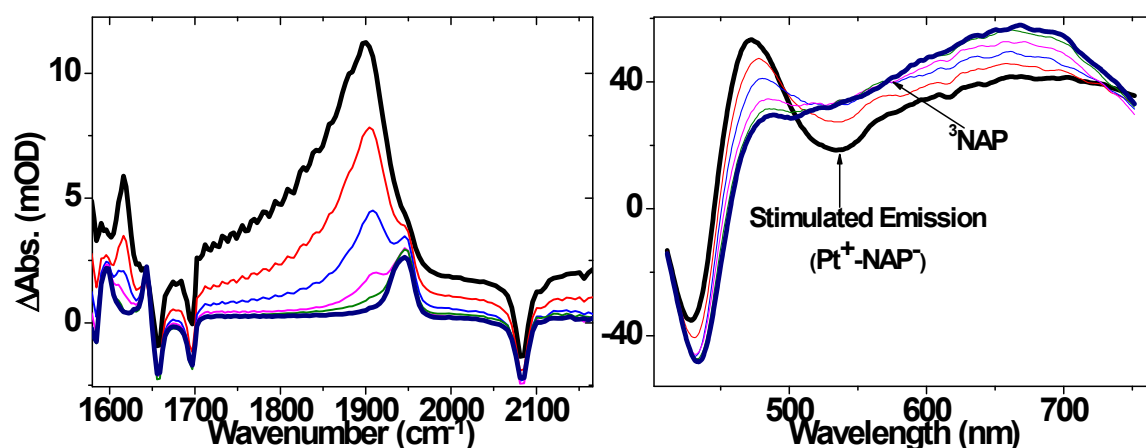


Figure S11a. Ultrafast TRIR (left) and TA (right) spectra at representative delay times for **1** in MeCN and at R.T. The delay times are 1.5, 3, 6, 12, 24 and 50 ps (colors black, red, blue, magenta, olive, navy) for TRIR and 1.4, 3, 6, 15, 30 and 60 ps for TA (same color order).

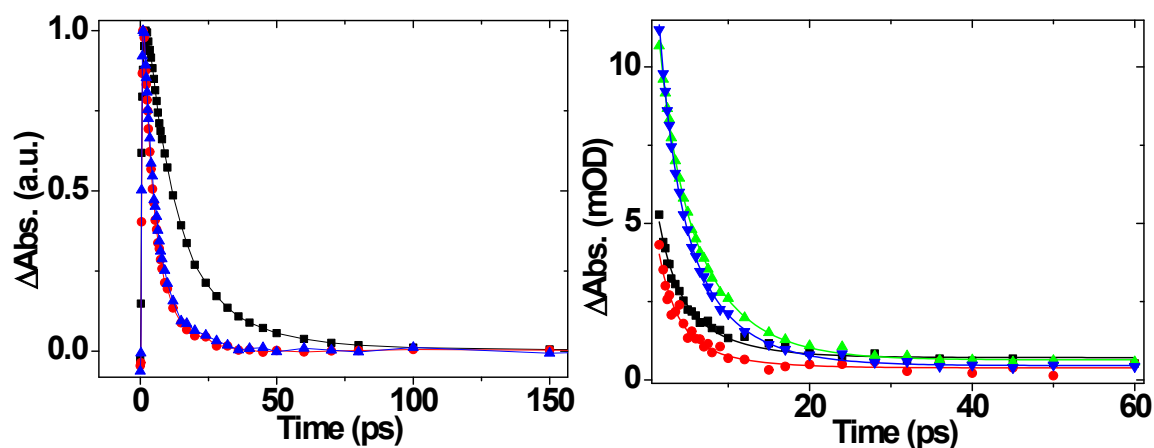


Figure S11b. TRIR kinetics for **1** in MeCN. The left graph shows a comparison of the decay of the $\text{C}\equiv\text{C}$ stretch in the CT state (1908 cm^{-1}) for **1** in CH_2Cl_2 (black squares), in MeCN at R.T. (red circles) and in MeCN at 43°C (blue triangles). There is no temperature dependence on these kinetics on this temperature scale. It is evident from the graph that the decay of CT state is faster in MeCN than in CH_2Cl_2 . TRIR kinetics (right) at 1613 cm^{-1} (black squares), 1550 cm^{-1} (red circles), 1908 cm^{-1} (green triangles) and 1896 cm^{-1} (blue inverted triangles) are shown on the right, globally fitted with a triple exponential function + constant with $\tau_1 \approx 2.0 \pm 0.2$ ps and $\tau_2 \approx 6.3 \pm 0.5$ ps and $\tau_3 \approx 60 \pm 5$ ps.

Computational Details

Upon convergence vibrational frequencies within the harmonic approximation were calculated to check whether a local minimum was found and to compare with the IR spectra. We note that for compound **3** small imaginary frequencies were found ($<10\text{cm}^{-1}$). These could be due to remaining inaccuracies in the quadrature or the geometry being a genuine transition state. This was investigated further by distorting the molecule in the direction of the imaginary frequency (a twist of the trans non-phosphine ligands) and re-optimizing. The same geometry was obtained and it was therefore decided that the imaginary frequency was caused by remaining inaccuracies in the quadratures used, a common problem for DFT-based methods, and the structures were deemed to be minima. For all structures deemed converged to a minimum, a UV-VIS spectrum was calculated using TD-DFT for 100 states.

Some initial analysis on our calculations was done using the Gausssum programme v. 2.2.5.⁶ Calculated IR spectra were generated using in-house developed software. We scaled the frequencies by 0.982 for the fingerprint region and by 0.966 for the acetylide region to account for anharmonicity and electronic effects not included in our calculations.⁷⁻¹¹

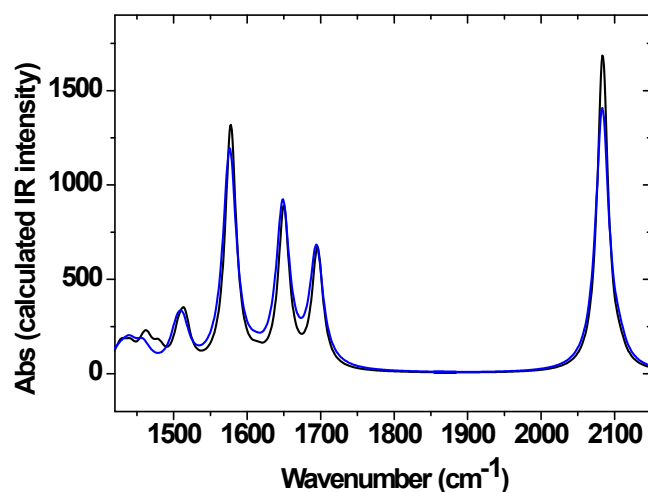
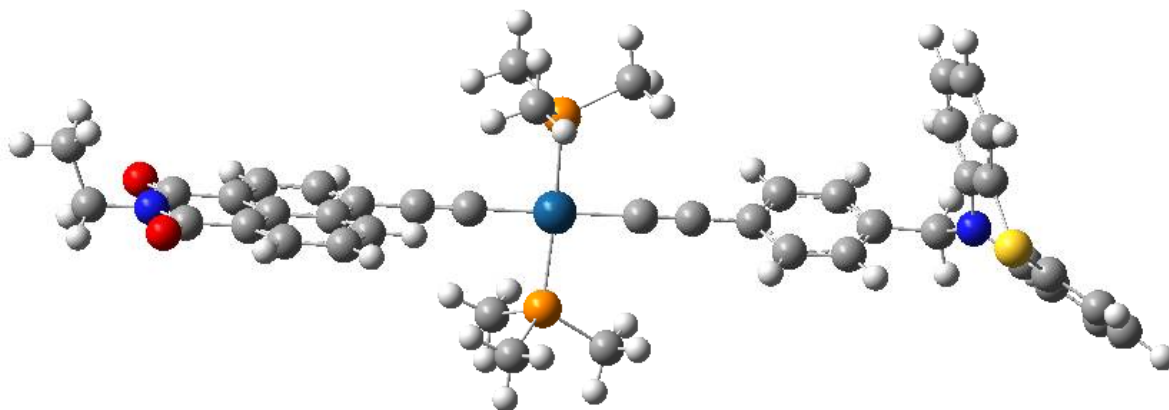


Figure S12. Calculated singlet ground state IR spectra for **2** with the full alkyl and n-Butyl chains (black) and the corresponding truncated structure (blue) where the C_8H_{17} tail is replaced by C_2H_5 and the Butyl chains are replaced by Methyl groups. Apart from slight changes in the calculated intensity, the band positions match well.

1 – NAP-Pt-PTZ in CH₂Cl₂, SINGLET:



SMILES : CCN1C(=O)c2cccc3c2c(ccc3C#C[Pt](C#Cc4ccc(cc4)CN5
c6cccc6Sc7c5cccc7)([P](C)(C)C)[P](C)(C)C)C1=O
Formula : C₄₃H₄₂N₂O₂P₂PtS
Charge : 0
Multiplicity : 1
Dipole : 7.3061 Debye
Energy : -3124.77521971 a.u.
Number of
imaginary
frequencies : 0

Cartesian Co-ordinates (XYZ format)

93

Pt	-1.07416105	-0.59423643	-0.59818518
P	-1.21857762	-2.71359420	0.42556408
C	0.34262064	-3.62529159	0.72204387
C	-2.01741385	-2.65322542	2.07656336
C	-2.24433088	-3.89408851	-0.53450364
P	-1.05954194	1.52876639	-1.62350535
H	0.85210806	-3.79381204	-0.22667749
H	0.99733949	-3.03127623	1.35931957
H	0.13052778	-4.58370161	1.20167828
S	9.27931213	1.58271778	2.33976173
H	-3.00834179	-2.20972276	1.97746491
H	-2.10382485	-3.65712118	2.49886060
H	-1.41994357	-2.03130603	2.74484038
H	-2.32453561	-4.84914970	-0.01016904
H	-3.23758340	-3.46854806	-0.67818439
H	-1.78796160	-4.05653143	-1.51210690
C	-2.03725815	1.57476509	-3.17568278
C	-1.81465304	2.82966137	-0.57231903
C	0.56282896	2.23326135	-2.10139561
H	-1.59579372	0.89052635	-3.90187144
H	-3.05668664	1.25142848	-2.96456599
H	-2.04936624	2.58490729	-3.59170461
H	-1.23425651	2.93589854	0.34546712
H	-1.83399940	3.78595376	-1.10018051
H	-2.83089495	2.53286982	-0.31239095
H	0.42376837	3.21357441	-2.56326818
H	1.19384670	2.32879472	-1.21795523
H	1.05903292	1.56301308	-2.80314946
C	0.94049722	-0.70699573	-0.67865598

C	2.16190314	-0.76815909	-0.71909803
C	-3.09161830	-0.47622076	-0.50905615
C	-4.31471014	-0.40708113	-0.46002105
C	-5.72979593	-0.33086991	-0.40877035
C	-6.50818920	-0.86759192	-1.43702233
C	-6.39809227	0.30082911	0.70157802
C	-7.90440702	-0.80277658	-1.40772843
H	-6.01258707	-1.34314823	-2.27397394
C	-7.82315159	0.35595968	0.71510512
C	-5.69153023	0.87180215	1.78636599
C	-8.56884289	-0.20159754	-0.35104671
H	-8.48728466	-1.22530985	-2.21668530
C	-8.48828125	0.97734100	1.80105674
C	-6.35880661	1.47143662	2.83431768
H	-4.60917997	0.82833523	1.77732921
C	-7.76274490	1.52612150	2.84265280
H	-5.80087185	1.90353227	3.65626311
H	-8.29587173	1.99543941	3.65968561
C	-10.04229450	-0.14884928	-0.34706274
C	-9.96763992	1.04505002	1.83199096
N	-10.65335846	0.45930660	0.76140559
O	-10.72507381	-0.60683167	-1.25283539
O	-10.58178043	1.58174372	2.74282575
C	-12.12979507	0.51001066	0.78591251
C	3.58716130	-0.83039486	-0.75799912
C	4.35626650	-0.63751686	0.40783951
C	4.27632809	-1.07931006	-1.96000636
C	5.74329853	-0.69180083	0.36959150
H	3.84977746	-0.44273654	1.34599018
C	5.66596508	-1.12818134	-1.98939955
H	3.71095514	-1.22753859	-2.87259197
C	6.42060804	-0.93632966	-0.82938844
H	6.31162357	-0.53407884	1.27943230
H	6.17003059	-1.31639564	-2.93252993
C	7.93201494	-1.07301044	-0.86804712
H	8.19234276	-2.06212544	-0.48746899
H	8.28197575	-1.03975630	-1.90839362
C	9.82028008	-0.50896215	0.63804132
C	8.45152283	1.27910340	-0.26430368
C	10.26973057	0.21653904	1.75648236
C	8.76033688	2.20430326	0.74816447
C	10.58304691	-1.60577118	0.21338935
C	11.43225193	-0.15018325	2.42938066
H	11.76047134	0.43558720	3.28024340
H	10.29328346	-2.16139412	-0.66837853
C	12.15495872	-1.27031481	2.02228713
C	11.72549248	-1.99228406	0.91286838
H	13.04776478	-1.56434119	2.56088376
H	12.28779888	-2.85370326	0.57147938
C	8.61347771	3.57300997	0.53778541
C	7.97767687	1.76977038	-1.48755050
H	8.87572479	4.26400280	1.33056474
H	7.73679686	1.08623815	-2.28956127
C	8.11564159	4.04512930	-0.67530423
C	7.79824495	3.13810277	-1.68233836
H	7.98327065	5.10936069	-0.82909632
H	7.41654158	3.49112630	-2.63339019
N	8.63026524	-0.10521939	-0.01704137
H	-12.42886734	0.46225706	1.83080018
H	-12.48295212	-0.38073358	0.27103928
C	-12.68617916	1.77006161	0.12433202
H	-12.38849831	1.82379913	-0.92485064
H	-13.77839661	1.75742137	0.16826591
H	-12.33539867	2.66767406	0.63765359

TD-DFT

Table S2. Detailed breakdown of transitions for **1** in the singlet manifold in CH₂Cl₂ from a TD-DFT calculation for all transitions with $f > 0.04$

No	Energy (cm ⁻¹)	Wavelength (nm)	Osc. Strength	Major contribs
1	21584	463.32	0.1204	H-1->LUMO (56%), HOMO->LUMO (38%)
3	22734	439.88	0.2276	H-3->LUMO (10%), H-2->LUMO (78%)
4	24623	406.12	0.3257	H-3->LUMO (82%), H-2->LUMO (14%)
13	32612	306.63	0.2314	H-1->L+2 (52%), H-1->L+4 (27%)
14	33763	296.18	0.4376	H-1->L+1 (64%)
16	34117	293.11	0.1308	H-3->L+2 (14%), H-2->L+1 (21%), H-2->L+2 (43%)
18	34379	290.88	0.0453	HOMO->L+1 (26%), HOMO->L+6 (48%)
23	35303	283.26	0.3462	H-2->L+1 (35%), H-2->L+2 (12%), H-1->L+3 (10%)
25	35557	281.24	0.0537	H-14->LUMO (16%), H-13->LUMO (22%), H-1->L+2 (16%), H-1->L+4 (16%)
29	36131	276.77	0.0748	H-3->L+2 (18%), H-2->L+4 (35%), H-2->L+5 (13%)
34	36859	271.30	0.1092	H-3->L+2 (12%), H-3->L+4 (36%), H-3->L+5 (12%)
38	37441	267.09	0.0401	H-15->LUMO (18%), H-3->L+1 (10%), H-3->L+3 (26%), H-2->L+3 (24%)
40	38316	260.98	0.1939	H-1->L+6 (41%), H-1->L+7 (34%), HOMO->L+11 (11%)
41	38996	256.44	0.2372	H-15->LUMO (18%), H-3->L+3 (55%)
42	39101	255.75	0.042	HOMO->L+11 (44%)
43	39317	254.35	0.0489	H-3->L+2 (12%), H-3->L+4 (10%), H-1->L+6 (14%), H-1->L+8 (16%), HOMO->L+11 (10%)
47	39889	250.69	0.0639	H-5->L+1 (10%), H-5->L+2 (61%), H-5->L+4 (20%)
48	40005	249.97	0.199	H-4->L+1 (13%), H-4->L+2 (41%), H-4->L+4 (17%)
49	40282	248.25	0.1189	H-4->L+2 (11%), H-4->L+5 (29%), HOMO->L+9 (30%), HOMO->L+13 (12%)
51	40380	247.65	0.0625	H-4->L+5 (13%), HOMO->L+9 (52%)
58	41460	241.19	0.0481	H-4->L+5 (10%), HOMO->L+10 (14%), HOMO->L+13 (61%)
62	42205	236.94	0.0497	H-5->L+4 (11%), H-3->L+9 (45%), H-2->L+10 (12%)
79	44178	226.36	0.1096	H-18->LUMO (32%), H-7->L+1 (24%), H-2->L+12 (10%)
81	44287	225.80	0.0614	H-18->LUMO (22%), H-11->L+1 (33%), H-7->L+3 (10%)
83	44675	223.84	0.1198	H-21->LUMO (11%), H-20->LUMO (16%), H-9->L+2 (10%), H-7->L+1 (15%)
92	45807	218.31	0.0479	H-13->L+2 (34%), H-13->L+4 (24%)
93	45824	218.23	0.126	H-8->L+1 (12%), H-8->L+2 (39%)
96	46425	215.40	0.0672	H-11->L+1 (13%), H-9->L+3 (18%), H-7->L+3 (41%)

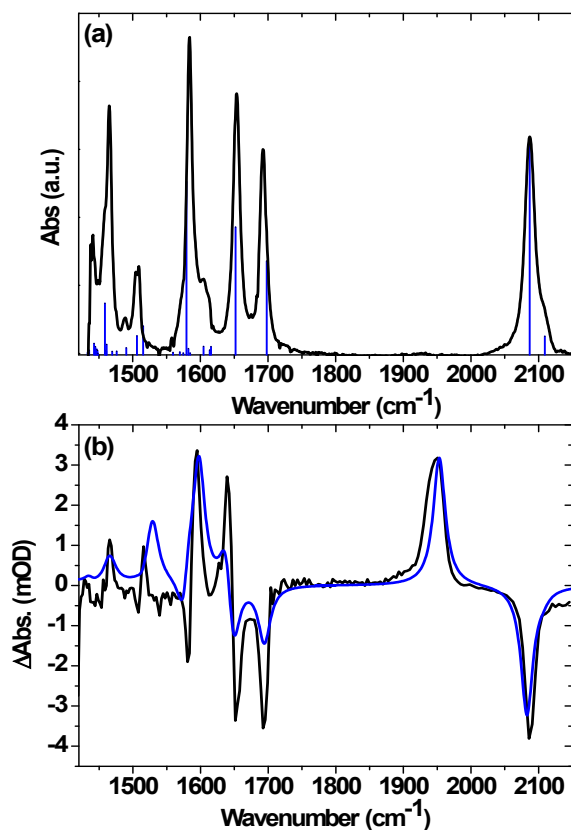


Figure S13. FTIR (a) and late-time TRIR (b) spectra (at 3 ns) for **1** in CH₂Cl₂ showing correspondence between experimental (black lines) and calculated (blue lines and sticks) data. The positions of the calculated bands in both panels were scaled by 0.982 in the fingerprint region and 0.966 in the acetylide region to account for anharmonicity and interactions not included in our calculations.^{37,75-77}

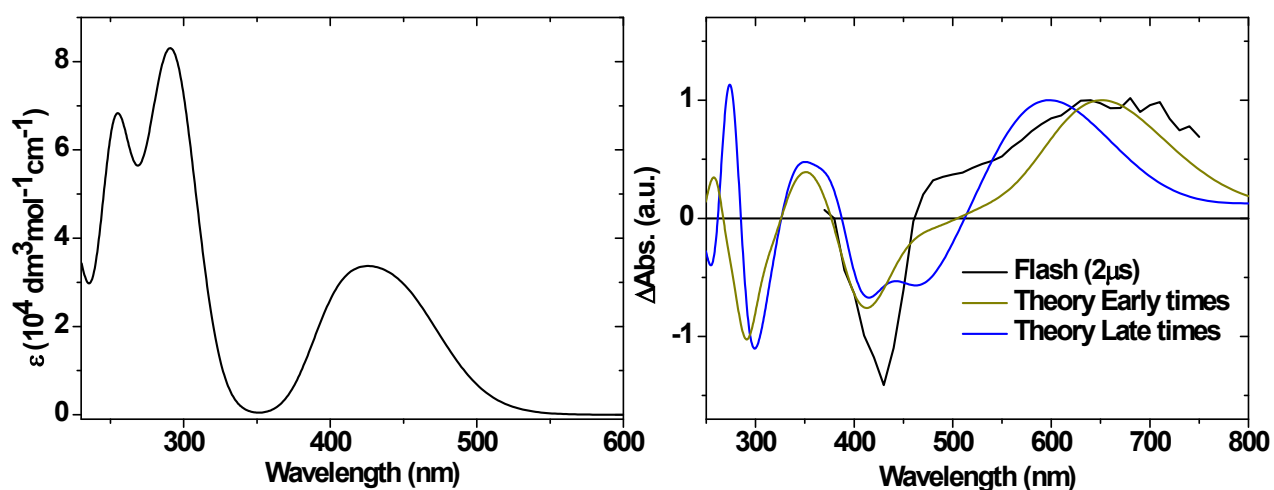
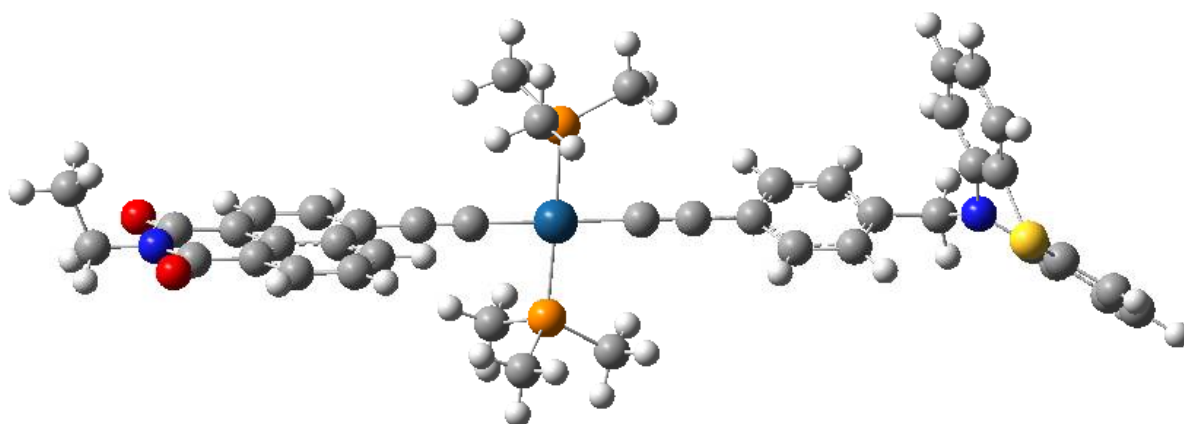


Figure S14. Calculated singlet UV-vis spectrum (left) and TA spectra (right) for ‘early times’ (dark yellow) and ‘late-times’ (blue), overlaid with the flash photolysis spectrum for **1** in CH₂Cl₂ 2 μ s after photo-excitation. The ‘late-time’ TA spectrum is obtained by subtracting the calculated singlet UV-Vis spectrum from the lowest triplet UV-Vis spectrum. The ‘early-time’ TA is calculated by subtracting the singlet UV-Vis spectrum from the triplet UV-Vis spectrum, the latter calculated with the starting singlet geometry, i.e. assuming there is no time for intramolecular re-organisation, as a representation of the CT state.

1 – NAP-Pt-PTZ in CH₂Cl₂, TRIPLET (T₁):



SMILES	:	CCN1C(=O)c2cccc3c2c(ccc3C#C[Pt](C#Cc4ccc(cc4)CN5c6ccc6Sc7e5cccc7)([P](C)(C)C)[P](C)(C)C)C1=O
Formula	:	C ₄₃ H ₄₂ N ₂ O ₂ P ₂ PtS ³
Charge	:	0
Multiplicity	:	3
Dipole	:	7.3061 Debye
Energy	:	-3124.70464043 a.u.
Number of imaginary frequencies	:	0

Cartesian Co-ordinates (XYZ format)

93

Pt	-1.08519149	-0.57017380	-0.57640815
P	-1.20597816	-2.69966197	0.44439870
C	0.36546198	-3.59742904	0.72185701
C	-1.99008977	-2.64509320	2.10200167
C	-2.23202562	-3.88041615	-0.51393104
P	-1.05334663	1.56287932	-1.59584999
H	0.86645627	-3.75961637	-0.23237643
H	1.02137649	-3.00014257	1.35465837
H	0.16444419	-4.55849266	1.20087147
S	9.29222488	1.52504146	2.34237432
H	-2.98655939	-2.21139288	2.01469016
H	-2.06265903	-3.64989758	2.52460790
H	-1.39183283	-2.01776385	2.76440358
H	-2.29687166	-4.84022236	0.00363046
H	-3.23158336	-3.46490169	-0.64290839
H	-1.78542840	-4.03053617	-1.49793589
C	-2.04187846	1.62546813	-3.13995528
C	-1.78481698	2.86278892	-0.52786815
C	0.57464272	2.24693894	-2.08001924
H	-1.61789751	0.93391472	-3.86954689
H	-3.06629562	1.32154477	-2.92384100
H	-2.03833556	2.63594866	-3.55510759
H	-1.19731379	2.95251632	0.38711083
H	-1.79345298	3.82370830	-1.04741454
H	-2.80403066	2.57993793	-0.26363948
H	0.44391370	3.23348331	-2.53083348
H	1.21422362	2.32511783	-1.20119691
H	1.05486894	1.57721484	-2.79320574
C	0.92745334	-0.68378049	-0.66577041

C	2.14833403	-0.74699277	-0.71233368
C	-3.08593154	-0.45427114	-0.47774962
C	-4.32451534	-0.38725659	-0.41488022
C	-5.70622873	-0.31787404	-0.34971613
C	-6.50183010	-0.93665105	-1.39567316
C	-6.39131403	0.35980195	0.74262577
C	-7.85885906	-0.90099400	-1.38369727
H	-5.97258663	-1.43461096	-2.19919753
C	-7.82503223	0.38465616	0.73994356
C	-5.72036505	0.98538500	1.79437518
C	-8.55228424	-0.23911412	-0.31324106
H	-8.44698811	-1.36212349	-2.16487050
C	-8.51724339	1.03219318	1.78182936
C	-6.42891645	1.62959075	2.82920027
H	-4.63746166	0.97190970	1.81016886
C	-7.80675364	1.65856433	2.83100486
H	-5.87626410	2.10635471	3.63067770
H	-8.36604404	2.14855909	3.61621594
C	-10.00842190	-0.21526161	-0.32536942
C	-9.98606777	1.06744134	1.79609823
N	-10.64697075	0.42483976	0.74581748
O	-10.66976833	-0.73279911	-1.23061025
O	-10.62357044	1.63026106	2.68501687
C	-12.12282753	0.44059643	0.75092876
C	3.57284617	-0.81366765	-0.75995451
C	4.34896898	-0.62664020	0.40193194
C	4.25272894	-1.06178939	-1.96732175
C	5.73543358	-0.68654829	0.35488892
H	3.84889197	-0.43251780	1.34360063
C	5.64179230	-1.11527121	-2.00548744
H	3.68092155	-1.20537031	-2.87658358
C	6.40398645	-0.93002987	-0.84919578
H	6.31017494	-0.53411078	1.26148200
H	6.13942909	-1.30206227	-2.95223069
C	7.91459608	-1.07302046	-0.89859146
H	8.17152023	-2.06951165	-0.53522396
H	8.25865555	-1.02539849	-1.94030464
C	9.81384087	-0.54232818	0.60534072
C	8.44931889	1.26653051	-0.26172721
C	10.27281284	0.16340774	1.73246050
C	8.76783085	2.17410731	0.76357430
C	10.56883430	-1.63588572	0.15916847
C	11.43724251	-0.21935165	2.39301801
H	11.77299595	0.35138091	3.25112200
H	10.27153587	-2.17611217	-0.72962981
C	12.15226078	-1.33633423	1.96428382
C	11.71325779	-2.03874850	0.84607893
H	13.04661465	-1.64301503	2.49315453
H	12.26955700	-2.89730310	0.48806462
C	8.62635803	3.54662204	0.57552177
C	7.97162437	1.77849865	-1.47467530
H	8.89597034	4.22382307	1.37766743
H	7.72360182	1.10888457	-2.28626871
C	8.12454033	4.04008389	-0.62739140
C	7.79777718	3.15058279	-1.64698720
H	7.99651241	5.10721684	-0.76372987
H	7.41308403	3.52039528	-2.59041882
N	8.62211514	-0.12243727	-0.03663803
H	-12.43352509	0.44118837	1.79352117
H	-12.44928646	-0.48337796	0.27813783
C	-12.69957352	1.65125728	0.01806731
H	-12.38838768	1.65725863	-1.02858698
H	-13.79185104	1.61617196	0.04888929
H	-12.37519073	2.58164835	0.48876911

TD-DFT

Table S3. Detailed breakdown of transitions for **1** in the triplet manifold in CH₂Cl₂ from a TD-DFT calculation for all transitions with $f > 0.04$

No.	Energy (cm ⁻¹)	Wavelength (nm)	Osc. Strength	Major contribs
3	8192	1220.67	0.09	H-2(β)->LUMO(β) (51%), H-1(β)->LUMO(β) (46%)
9	15643	639.25	0.1501	HOMO(α)->LUMO(α) (44%), H-12(β)->LUMO(β) (18%), H-5(β)->LUMO(β) (20%)
11	17338	576.77	0.1929	HOMO(α)->LUMO(α) (19%), H-12(β)->LUMO(β) (40%), H-7(β)->LUMO(β) (12%)
21	23333	428.58	0.0597	HOMO(α)->L+1(α) (24%), HOMO(α)->L+2(α) (58%)
22	23759	420.90	0.2051	HOMO(α)->L+9(α) (40%), H-16(β)->LUMO(β) (32%)
28	25869	386.57	0.1156	HOMO(α)->L+9(α) (12%), H-18(β)->LUMO(β) (24%), H-17(β)->LUMO(β) (19%), H-16(β)->LUMO(β) (17%), H-2(β)->L+1(β) (10%)
37	28563	350.11	0.0501	H-17(β)->LUMO(β) (21%), H-5(β)->L+1(β) (49%)
38	28933	345.63	0.0463	H-18(β)->LUMO(β) (39%), H-17(β)->LUMO(β) (32%)
41	29743	336.22	0.0446	H-23(β)->LUMO(β) (14%), H-22(β)->LUMO(β) (51%), H-18(β)->LUMO(β) (10%)
57	32940	303.58	0.2937	H-2(α)->L+1(α) (36%), H-2(α)->L+2(α) (16%), H-1(β)->L+2(β) (28%)
63	34234	292.11	0.0406	H-3(α)->LUMO(α) (24%), HOMO(α)->L+16(α) (12%), H-12(β)->L+1(β) (29%)
64	34331	291.28	0.0641	H-1(α)->L+2(α) (10%), H-1(α)->L+5(α) (29%), HOMO(β)->L+6(β) (12%), HOMO(β)->L+7(β) (15%)
67	34723	287.99	0.0528	H-1(α)->L+6(α) (26%), HOMO(β)->L+8(β) (21%)
69	34825	287.15	0.1634	H-3(α)->L+1(α) (14%), H-2(β)->L+2(β) (41%)
74	35131	284.65	0.1586	H-3(α)->LUMO(α) (13%), HOMO(α)->L+16(α) (11%)
75	35417	282.35	0.1015	H-12(β)->L+1(β) (10%), H-11(β)->L+1(β) (21%)
77	35749	279.73	0.1323	HOMO(α)->L+15(α) (16%), H-11(β)->L+1(β) (15%)
80	35955	278.13	0.0809	H-2(α)->L+2(α) (16%), H-28(β)->LUMO(β) (16%), H-1(β)->L+3(β) (12%)
94	37023	270.10	0.2602	H-3(α)->L+2(α) (32%), H-2(β)->L+3(β) (22%)
97	37419	267.25	0.0619	H-4(α)->L+3(α) (14%), H-2(α)->L+3(α) (51%)

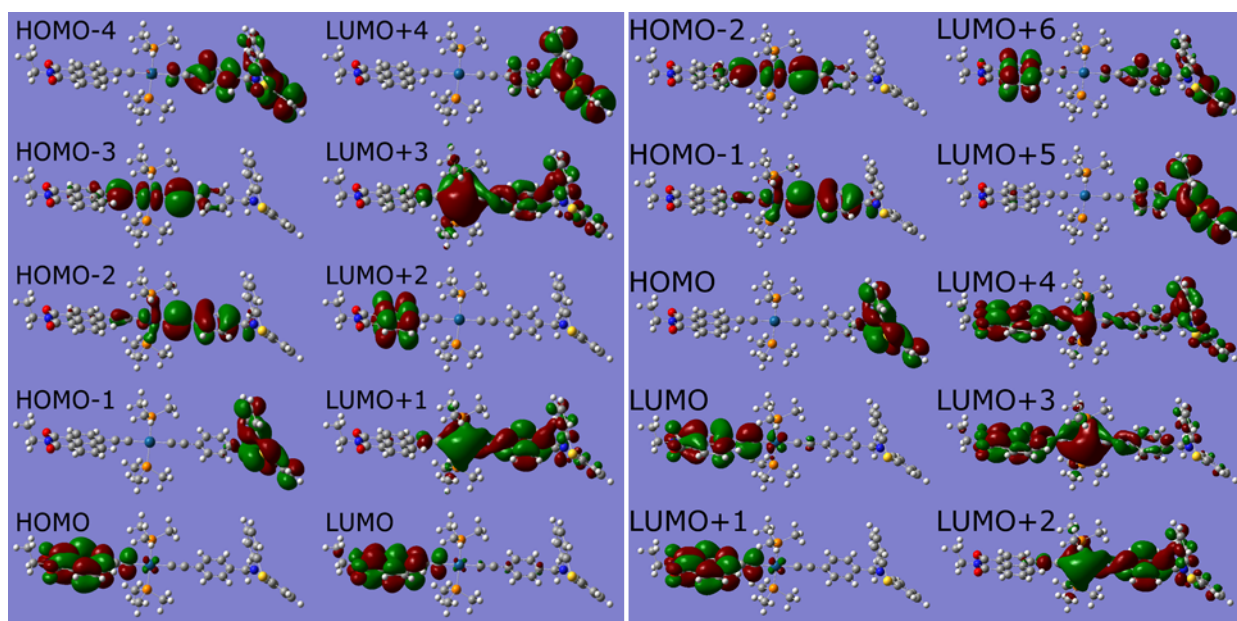


Figure S15. Alpha-manifold (left) and beta-manifold (right) triplet molecular orbitals for **1**. Both HOMO and LUMO are located on the NAP moiety in the alpha manifold, as expected from spectroscopic data indicating ³NAP as the lowest-lying triplet state.

1 – NAP-Pt-PTZ in CH₂Cl₂, T₂, first triplet excited state:

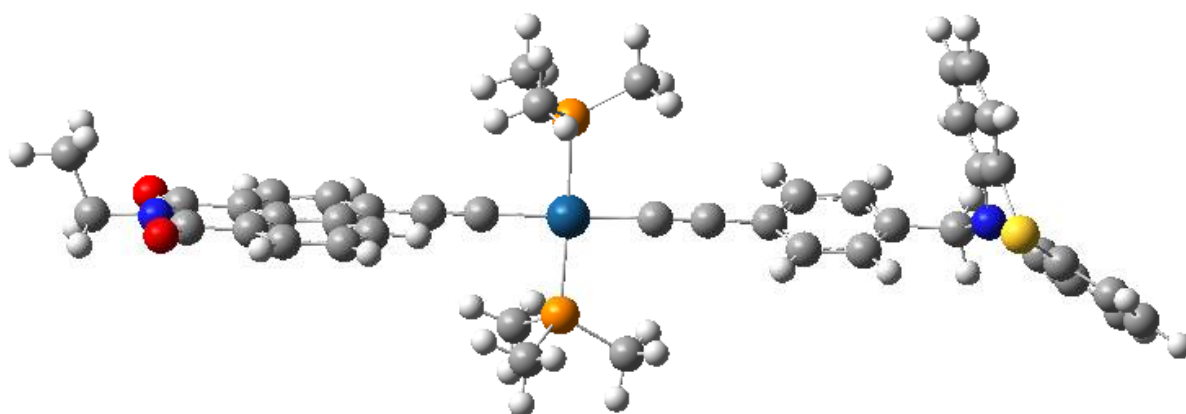


Table S4. Detailed breakdown of transitions for **1** from the first triplet excited state, T², in CH₂Cl₂ from a TD-DFT calculation for all transitions with *f* > 0.04

No.	Energy (cm ⁻¹)	Wavelength (nm)	Osc. Strength	Major contribs
2	4914.37	2034.85	0.042	H-2(β)->LUMO(β) (32%), H-1(β)->LUMO(β) (61%)
3	6331.5	1579.41	0.112	H-2(β)->LUMO(β) (62%), H-1(β)->LUMO(β) (35%)
4	9948.92	1005.13	0.0421	HOMO(α)->LUMO(α) (22%), H-5(β)->LUMO(β) (73%)
9	13979.3	715.344	0.1598	HOMO(α)->LUMO(α) (46%), H-11(β)->LUMO(β) (23%), H-5(β)->LUMO(β) (18%)
10	14866.5	672.653	0.0623	HOMO(α)->L+2(α) (70%)
12	15480.3	645.982	0.1371	HOMO(α)->LUMO(α) (11%), HOMO(α)->L+2(α) (16%), H-11(β)->LUMO(β) (64%)
20	20346.3	491.49	0.0469	HOMO(α)->L+9(α) (31%), H-18(β)->LUMO(β) (17%), H-17(β)->LUMO(β) (10%), H-16(β)->LUMO(β) (20%)
22	21903.7	456.543	0.2527	HOMO(α)->L+9(α) (41%), H-16(β)->LUMO(β) (41%)
25	24186.3	413.457	0.1749	HOMO(α)->L+9(α) (14%), H-18(β)->LUMO(β) (40%), H-17(β)->LUMO(β) (17%), H-16(β)->LUMO(β) (15%)
37	27927.9	358.064	0.0533	H-21(β)->LUMO(β) (56%)
50	32241.4	310.16	0.0403	H-6(β)->L+1(β) (84%)
54	32652.8	306.253	0.0563	HOMO(α)->L+13(α) (85%)
56	32936.7	303.613	0.3432	H-2(α)->L+1(α) (26%), H-1(β)->L+2(β) (37%), H-1(β)->L+3(β) (16%)
59	33488.4	298.611	0.0914	HOMO(α)->L+16(α) (27%), HOMO(α)->L+17(α) (19%), H-11(β)->L+1(β) (15%)
65	33930.4	294.721	0.0578	H-2(α)->LUMO(α) (71%)
67	34166.7	292.683	0.0932	H-1(α)->L+5(α) (32%), HOMO(β)->L+7(β) (27%)
70	34556.3	289.383	0.1016	H-1(α)->L+6(α) (28%), HOMO(β)->L+8(β) (24%)
72	34778.9	287.531	0.0463	H-3(α)->LUMO(α) (25%), H-3(α)->L+1(α) (17%), H-11(β)->L+1(β) (10%)
74	35041.8	285.373	0.1697	H-2(β)->L+2(β) (26%), H-1(β)->L+3(β) (13%)
75	35076.5	285.091	0.0613	H-3(α)->L+1(α) (24%), H-2(β)->L+2(β) (21%)
78	35533.8	281.422	0.1427	HOMO(β)->L+3(β) (37%)
79	35575.7	281.09	0.192	H-1(α)->L+3(α) (20%), HOMO(β)->L+3(β) (11%)
82	35907.2	278.495	0.0719	H-2(α)->L+3(α) (10%), H-14(β)->L+1(β) (12%)
96	37148.5	269.19	0.1143	H-3(α)->L+3(α) (15%), H-2(α)->L+2(α) (43%), H-2(β)->L+3(β) (12%)
97	37254.2	268.426	0.1972	H-3(α)->L+3(α) (24%), H-2(α)->L+2(α) (30%), H-2(β)->L+3(β) (20%)
98	37371.2	267.586	0.0463	H-2(α)->L+7(α) (13%), H-1(β)->L+10(β) (40%)

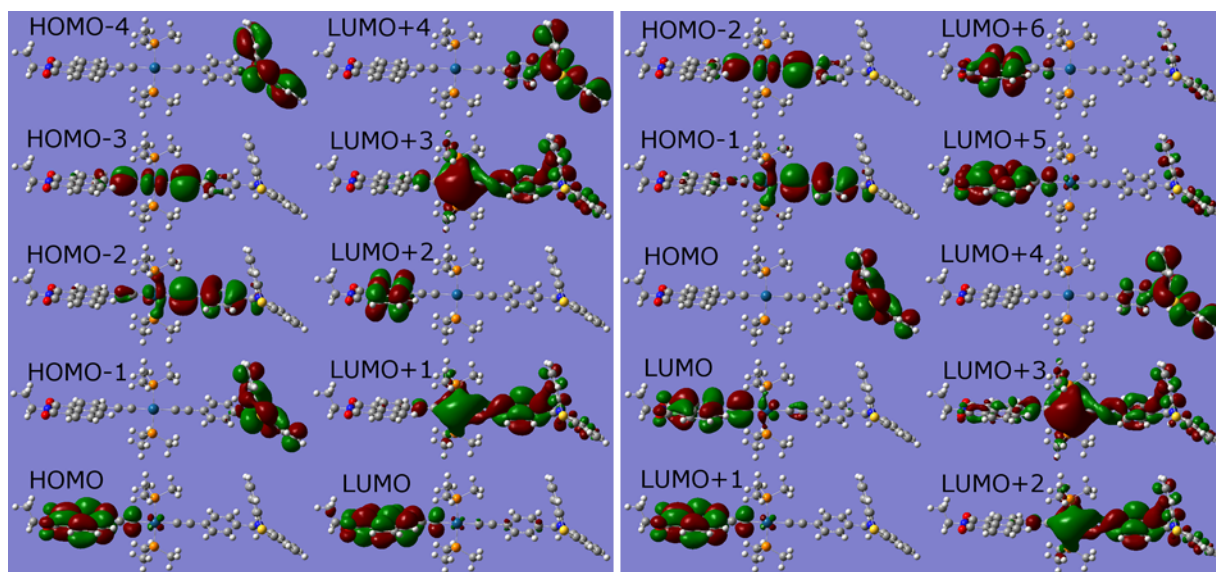
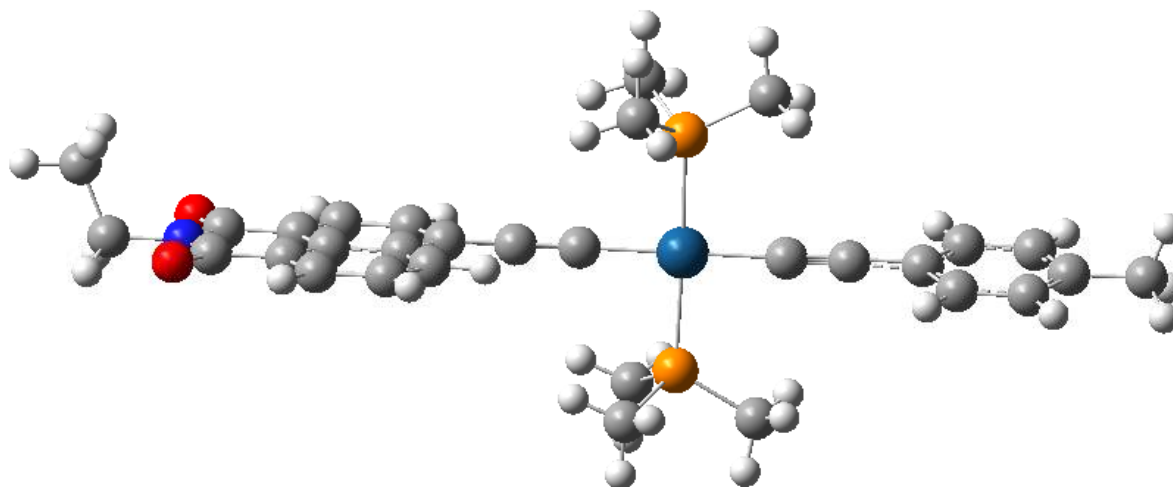


Figure S16. Alpha-manifold (left) and beta-manifold (right) triplet molecular orbitals for **1** in the first excited triplet state, T_2 .

2 – NAP-Pt-Ph in CH₂Cl₂, SINGLET:



SMILES	:	CCN1C(=O)c2cccc3c2c(ccc3C#C[Pt](C#Cc4ccc(cc4)C)([P](C)(C)C)[P](C)(C)C)C1=O
Formula	:	C ₃₁ H ₃₅ NO ₂ P ₂ Pt
Charge	:	0
Multiplicity	:	1
Dipole	:	7.4989 Debye
Energy	:	-2210.19962332 a.u.
Number of imaginary frequencies	:	1 ¹

Cartesian Co-ordinates (XYZ format)

72

Pt	-1.75028133	-0.00419824	-0.23164241
P	-1.71142542	2.34918427	-0.38056847
C	-3.30933309	3.23820877	-0.26555052
C	-0.67664605	3.12998414	0.91822994
C	-0.98629826	2.94442058	-1.95741320
P	-1.66319108	-2.35790467	-0.11057967
H	-3.97442198	2.89784575	-1.05899656
H	-3.78099298	3.01871467	0.69219553
H	-3.14591241	4.31450653	-0.35764331
H	0.33188668	2.71983242	0.86475492
H	-0.64144063	4.21329689	0.78136730
H	-1.09598756	2.90365005	1.89975893
H	-0.94233203	4.03594112	-1.97090280
H	0.01793631	2.53435659	-2.06566668
H	-1.59851754	2.59724832	-2.79106998
C	-0.91944861	-3.11393094	-1.60801685
C	-0.61705321	-2.96321964	1.27003837
C	-3.24275208	-3.26073647	0.10371274
H	-1.53606832	-2.87820387	-2.47662425
H	0.07587675	-2.69638824	-1.76114881
H	-0.85109669	-4.19863129	-1.49693155
H	-1.04338765	-2.63357782	2.21870375
H	-0.56104249	-4.05420017	1.25876963
H	0.38360393	-2.54248953	1.17002082
H	-3.05605960	-4.33660364	0.13796493
H	-3.72309852	-2.94117403	1.02843654
H	-3.91121817	-3.02857947	-0.72516257

¹ Imaginary frequency: -9cm⁻¹ deemed to be an artefact of quadrature used in integration grid (see main article).

C	-3.76215863	-0.01464898	-0.04175681
C	-4.98012257	-0.02572323	0.07403819
C	0.26486617	0.00697546	-0.42004594
C	1.48532617	0.01861131	-0.53662008
C	2.89668345	0.03537051	-0.67292213
C	3.49002743	-0.00697676	-1.93678725
C	3.75162482	0.09723781	0.48642597
C	4.87912035	0.00982513	-2.09364581
H	2.85377908	-0.05368339	-2.81158423
C	5.16634369	0.11527868	0.30679345
C	3.23934579	0.14196396	1.80461407
C	5.72077417	0.07048093	-0.99482292
H	5.31687069	-0.02371493	-3.08353639
C	6.01425648	0.17362429	1.44060612
C	4.08266735	0.19929317	2.89482164
H	2.16480875	0.13017669	1.94131958
C	5.47588634	0.21427581	2.71382642
H	3.67215443	0.23267083	3.89679480
H	6.14603758	0.25824502	3.56294298
C	7.18184233	0.08964686	-1.19136715
C	7.48593044	0.19288483	1.27360022
N	7.97725487	0.16976193	-0.03688234
O	7.70360518	0.04112914	-2.29673505
O	8.25452518	0.22965197	2.22376943
C	9.44315815	0.20302665	-0.21829720
C	-6.40159512	-0.04205558	0.21115452
C	-7.23281670	-0.47019985	-0.84246176
C	-7.02585793	0.37218124	1.40352535
C	-8.61589909	-0.48265913	-0.70380718
H	-6.78044415	-0.78908038	-1.77453661
C	-8.41036701	0.35349703	1.53120720
H	-6.41182566	0.71156818	2.22986603
C	-9.23462677	-0.07547508	0.48442942
H	-9.22804832	-0.81443679	-1.53687716
H	-8.86006927	0.68166184	2.46326709
C	-10.73542213	-0.12315603	0.63915843
H	-11.06531906	-1.11034107	0.98200512
H	-11.08379269	0.60874826	1.37137949
H	9.84804344	0.79406434	0.60033953
H	9.63122940	0.71693915	-1.15837193
C	10.06568527	-1.19232678	-0.23394252
H	9.66070175	-1.79056287	-1.05269849
H	11.14694786	-1.11172104	-0.37321317
H	9.88183022	-1.71204972	0.70858651
H	-11.24041653	0.07568838	-0.30914930

Table S5. Detailed breakdown of transitions for **2** in the singlet manifold in CH₂Cl₂ from a TD-DFT calculation for all transitions with $f > 0.04$

No.	Energy (cm ⁻¹)	Wavelength (nm)	Osc. Strength	Major contribs
1	21127.03	473.3272	0.1426	HOMO->LUMO (94%)
2	22678.05	440.9551	0.1584	H-2->LUMO (12%), H-1->LUMO (80%)
3	24432.32	409.294	0.3881	H-2->LUMO (81%), H-1->LUMO (15%)
8	32184.97	310.704	0.1598	HOMO->L+3 (87%)
11	33563.38	297.9438	0.2587	HOMO->L+1 (79%)
13	34613.52	288.9044	0.1404	H-2->L+3 (14%), H-1->L+1 (16%), H-1->L+3 (60%)
15	35236.99	283.7927	0.2375	H-1->L+1 (53%), H-1->L+3 (12%), HOMO->L+2 (23%)
17	35817.72	279.1914	0.0437	H-11->LUMO (12%), H-9->LUMO (22%), H-1->L+2 (17%), HOMO->L+2 (23%)
21	36667.83	272.7186	0.0638	H-2->L+1 (29%), H-2->L+3 (13%), HOMO->L+4 (13%)
23	36993.68	270.3164	0.0838	H-1->L+2 (15%), H-1->L+4 (10%), HOMO->L+4 (37%)
25	37530.85	266.4475	0.5125	H-2->L+4 (28%), H-1->L+4 (35%), HOMO->L+4 (22%)
27	38851.19	257.3924	0.2532	H-11->LUMO (21%), H-2->L+2 (50%)
30	40134.43	249.1627	0.0739	H-3->L+3 (90%)
37	42036.29	237.8897	0.056	H-2->L+6 (62%), H-1->L+7 (20%)
43	43678.45	228.9459	0.0435	H-15->LUMO (41%), H-5->L+1 (24%), H-1->L+8 (15%)
46	44226.91	226.1067	0.0903	H-7->L+1 (37%), H-5->L+2 (17%), H-1->L+8 (16%)
47	44595.51	224.2378	0.1447	H-15->LUMO (20%), H-6->L+3 (13%), H-5->L+1 (35%)
52	45806.16	218.3113	0.0439	H-4->L+1 (16%), H-4->L+3 (65%)
53	45835.19	218.173	0.0773	H-10->L+3 (78%)
59	46626.43	214.4706	0.1086	H-7->L+1 (20%), H-6->L+2 (26%), H-5->L+2 (21%)
68	48095.17	207.9211	0.1252	H-11->L+2 (12%), H-10->L+7 (10%), H-7->L+2 (28%), H-6->L+4 (13%)
69	48124.21	207.7956	0.1135	H-11->L+2 (14%), H-10->L+6 (10%), H-10->L+7 (10%), H-7->L+2 (26%), H-6->L+4 (16%)
72	48476.68	206.2848	0.0547	H-2->L+10 (15%), H-1->L+10 (66%)
75	48837.21	204.7619	0.0834	H-11->L+1 (15%), H-9->L+1 (26%), HOMO->L+11 (30%)
76	48889.63	204.5423	0.1067	H-12->L+1 (10%), H-11->L+1 (19%), H-1->L+9 (12%), HOMO->L+11 (38%)
80	49464.71	202.1643	0.142	H-11->L+1 (15%), H-11->L+2 (34%), H-7->L+2 (13%)
95	51361.74	194.6975	0.055	H-6->L+5 (25%), H-5->L+5 (10%), H-1->L+11 (27%)
96	51448.85	194.3678	0.1058	H-6->L+6 (11%), H-5->L+6 (15%), H-1->L+11 (33%)
97	51556.12	193.9634	0.0461	H-13->L+3 (39%), H-11->L+3 (15%)
100	51948.11	192.4998	0.0911	H-1->L+11 (11%), HOMO->L+12 (44%)

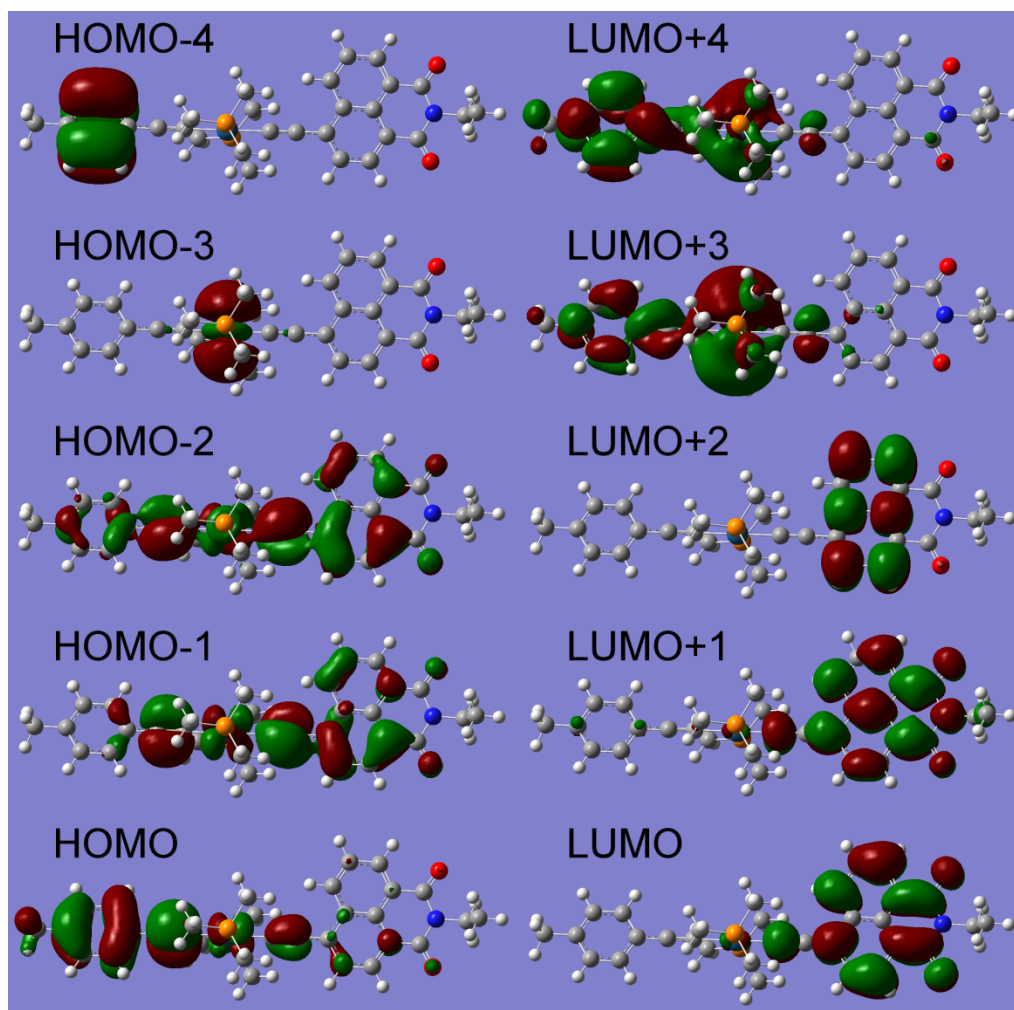
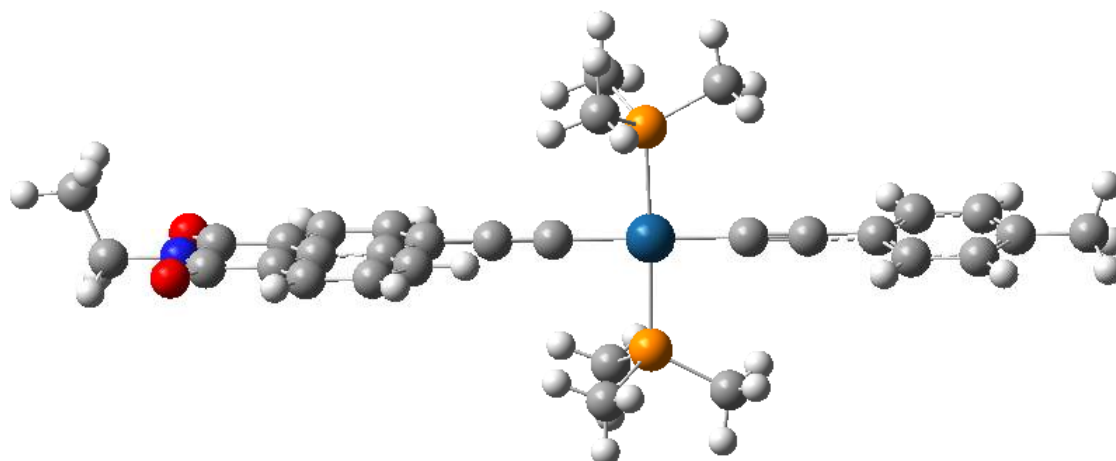


Figure S17. Singlet molecular orbitals for **2**. Referring to table S5, the major transitions in the ML/L'CT band are from delocalized densities around the bridge and phenyl ring to the NAP ligand.

3 – NAP-Pt-Ph in CH₂Cl₂, TRIPLET:



SMILES : CCN1C(=O)c2cccc3c2c(ccc3C#C[Pt](C#Cc4ccc(cc4)C)([P](C)(C)C)[P](C)(C)C)C1=O
 Formula : C₃₁H₃₅NO₂P₂Pt³
 Charge : 0
 Multiplicity : 3
 Dipole : 7.4989 Debye
 Energy : -2210.12911876 a.u.
 Number of imaginary frequencies : 1

Cartesian Co-ordinates (XYZ format)

72

Pt	-1.73512340	-0.00729492	-0.22131048
P	-1.73400998	2.35158467	-0.40706694
C	-3.34929705	3.21053267	-0.33271968
C	-0.73505282	3.16105390	0.90119863
C	-0.98914796	2.93251228	-1.97952759
P	-1.64797807	-2.36384201	-0.03536910
H	-3.99028254	2.85362840	-1.13859141
H	-3.83786893	2.98896790	0.61589277
H	-3.20146537	4.28871202	-0.42863449
H	0.28265625	2.77150202	0.86891967
H	-0.71865588	4.24347210	0.75477833
H	-1.16599345	2.93512225	1.87766087
H	-0.96675318	4.02421522	-2.01203156
H	0.02554257	2.54229403	-2.06145144
H	-1.57747638	2.55835271	-2.81861925
C	-0.87351722	-3.16170120	-1.49409068
C	-0.63088864	-2.92032337	1.38618851
C	-3.23340726	-3.25585365	0.17321134
H	-1.46742225	-2.94565225	-2.38334703
H	0.12885453	-2.75702381	-1.63556707
H	-0.81634337	-4.24321651	-1.35126543
H	-1.07743180	-2.55968070	2.31399560
H	-0.57462490	-4.01100159	1.41200137
H	0.37248746	-2.50383329	1.29512203
H	-3.04845428	-4.32994270	0.24823198
H	-3.73416567	-2.90417600	1.07506704
H	-3.88199830	-3.05268002	-0.67869437
C	-3.74615145	-0.02946663	-0.04464481
C	-4.96493912	-0.03869114	0.06145852
C	0.26456636	0.01651568	-0.39332801
C	1.50216937	0.03243878	-0.49647865
C	2.88199878	0.05159783	-0.61536312

C	3.48484635	0.04056753	-1.93650520
C	3.75318789	0.08318581	0.55160028
C	4.83079815	0.06057796	-2.11328435
H	2.81902242	0.01470004	-2.79075098
C	5.17208052	0.10708480	0.34531218
C	3.27461147	0.09297324	1.86266124
C	5.70610714	0.09625667	-0.97445518
H	5.27517557	0.05138948	-3.09875989
C	6.04162693	0.13763441	1.45312285
C	4.15906191	0.12287916	2.96015739
H	2.20506668	0.07717992	2.03288865
C	5.52366543	0.14405946	2.76827383
H	3.75352240	0.12892117	3.96545410
H	6.21600866	0.16630326	3.59873199
C	7.14581251	0.11925195	-1.19272351
C	7.49806404	0.16322139	1.26104486
N	7.96479034	0.16895545	-0.05621031
O	7.64296436	0.09849976	-2.32282019
O	8.28762054	0.18150698	2.20432663
C	9.42500305	0.20798521	-0.26774058
C	-6.38727474	-0.04683349	0.18388098
C	-7.21469402	-0.27788037	-0.93241870
C	-7.01486158	0.18209352	1.42357254
C	-8.59900951	-0.27983379	-0.80819643
H	-6.75853539	-0.45164526	-1.90024137
C	-8.40061378	0.17747720	1.53523862
H	-6.40271378	0.36770076	2.29866004
C	-9.22178459	-0.05540681	0.42570427
H	-9.20898056	-0.45712999	-1.68859231
H	-8.85391903	0.36113277	2.50438905
C	-10.72481632	-0.08971117	0.55874223
H	-11.08032417	-1.10911846	0.74656445
H	-11.06537533	0.53195727	1.38982451
H	9.84772205	0.76700121	0.56430161
H	9.59493351	0.75489575	-1.19292057
C	10.04490662	-1.18669403	-0.34710130
H	9.62450790	-1.75337195	-1.18047118
H	11.12397766	-1.10308194	-0.50166553
H	9.87543678	-1.74089193	0.57844269
H	-11.21360493	0.26110443	-0.35321718

TD-DFT

Table S6. Detailed breakdown of transitions for **2** in the triplet manifold in CH₂Cl₂ from a TD-DFT calculation for all transitions with $f > 0.04$

No.	Energy (cm ⁻¹)	Wavelength (nm)	Osc. Strength	Major contribs
2	7319.532	1366.208	0.0749	H-1(β)->LUMO(β) (48%), HOMO(β)->LUMO(β) (49%)
7	15659.36	638.5956	0.1454	HOMO(α)->LUMO(α) (45%), H-8(β)->LUMO(β) (19%), H-3(β)->LUMO(β) (20%)
9	17330.55	577.0156	0.1887	HOMO(α)->LUMO(α) (18%), HOMO(α)->L+2(α) (11%), H-8(β)->LUMO(β) (42%), H-5(β)->LUMO(β) (12%)
17	23403.14	427.293	0.2323	HOMO(α)->L+6(α) (40%), H-12(β)->LUMO(β) (36%)
22	25792.98	387.7024	0.1391	HOMO(α)->L+6(α) (17%), H-13(β)->LUMO(β) (41%), H-1(β)->L+1(β) (11%)
27	28512.7	350.7209	0.0696	H-3(β)->L+1(β) (60%)
29	29558.81	338.3086	0.0666	H-17(β)->LUMO(β) (16%), H-16(β)->LUMO(β) (65%)
39	32690.68	305.8976	0.0512	H-1(α)->L+1(α) (50%), HOMO(β)->L+2(β) (39%)
45	35020.84	285.5443	0.0517	HOMO(α)->L+11(α) (17%), H-25(β)->LUMO(β) (10%), H-11(β)->L+1(β) (30%), H-7(β)->L+1(β) (11%)
49	35441.05	282.1587	0.0474	H-8(β)->L+1(β) (11%), H-7(β)->L+1(β) (28%)
50	35677.38	280.2897	0.0501	H-2(α)->L+3(α) (16%), H-1(β)->L+4(β) (16%)

52	35899.18	278.5579	0.3043	H-2(α)->L+1(α) (35%), H-1(β)->L+2(β) (30%)
56	36282.3	275.6165	0.1182	HOMO(α)->L+11(α) (14%), H-20(β)->LUMO(β) (38%), H-19(β)->LUMO(β) (10%)
58	36675.9	272.6586	0.0553	H-25(β)->LUMO(β) (39%), H-23(β)->LUMO(β) (13%), H-11(β)->L+1(β) (17%)
63	37097.73	269.5583	0.0931	H-1(α)->L+2(α) (47%)
64	37126.76	269.3475	0.289	H-2(α)->L+3(α) (21%), H-1(α)->L+2(α) (15%), H-1(β)->L+4(β) (10%), HOMO(β)->L+3(β) (21%)
66	37605.86	265.916	0.3743	H-1(α)->L+3(α) (23%), HOMO(β)->L+3(β) (11%), HOMO(β)->L+4(β) (52%)
93	40757.9	245.3512	0.0679	H-4(α)->L+1(α) (48%), H-2(β)->L+2(β) (44%)

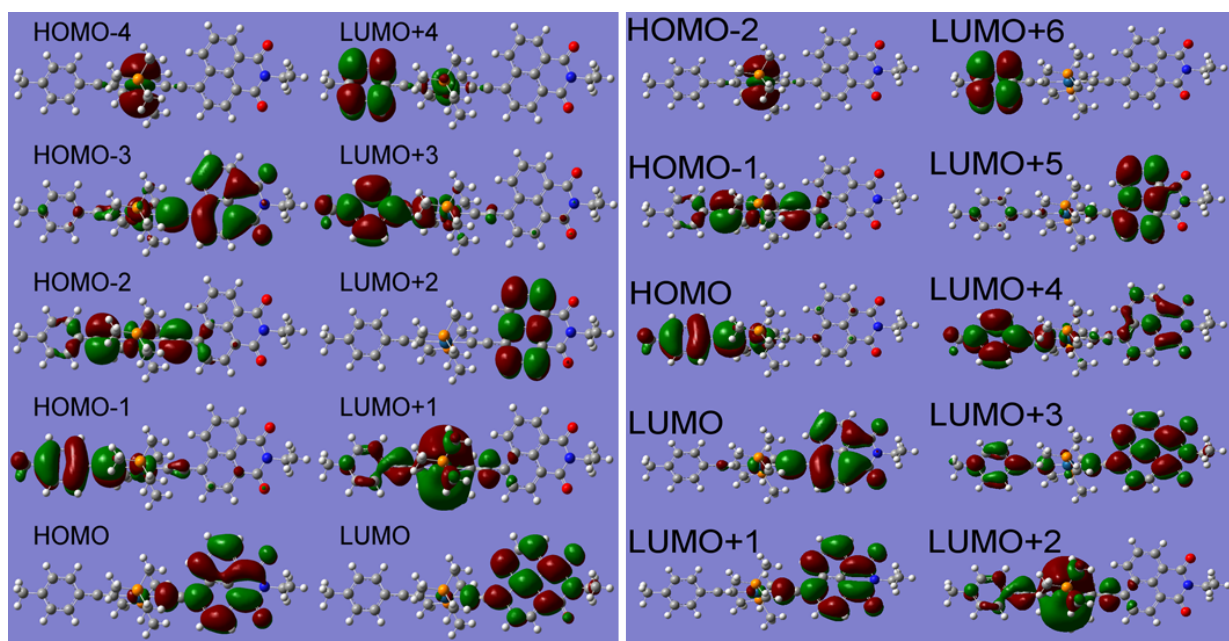


Figure S18. Alpha-manifold (left) and beta-manifold (right) triplet molecular orbitals for **2**. Similarly to figure S15, both HOMO and LUMO are located on the NAP moiety in the alpha-manifold, as expected from spectroscopic data indicating ^3NAP as the lowest-lying triplet state.

References

1. J. E. McGarrah, Y.-J. Kim, M. Hissler, R. Eisenberg, *Inorg. Chem.*, 2001, **40**, 4510–4511.
2. R. W. Murray, W. R. Heineman, and G. W. O'Dom, *Anal. Chem.*, 1967, **39**, 1666–68.
3. M. Krejčík, M. Daněk, and F. Hartl, *J. Electroanal. Chem. Interfacial Electrochem.*, 1991, **317**, 179–187.
4. G. Greetham, P. Burgos, Q. Cao, I. Clark, P. Codd, R. Farrow, M. George, M. Kogimtzis, P. Matousek, A. Parker, M. Pollard, D. Robinson, Z.-J. Xin, and M. Towrie, *Appl. Spectrosc.*, 2010, **64**, 1311–1319.
5. R. Schmidt, C. Tanielian, R. Dunsbach, and C. Wolff, *J. Photochem. Photobiol. A Chem.*, 1994, **79**, 11–17.
6. B. Mennucci and J. Tomasi, *J. Chem. Phys.*, 1997, **106**, 5151.
7. I. V. Sazanovich, M. A. H. Alamiry, A. J. H. M. Meijer, M. Towrie, E. S. Davies, R. D. Bennett, and J. A. Weinstein, *Pure Appl. Chem.*, 2013, **85**, 1331–1348.
8. K. K. Irikura, R. D. Johnson, and R. N. Kacker, *J. Phys. Chem. A*, 2005, **109**, 8430–7.
9. J. Baker, A. A. Jarzecki, and P. Pulay, *J. Phys. Chem. A*, 1998, **102**, 1412–1424.
10. M. D. Halls, J. Velkovski, and H. B. Schlegel, *Theor. Chem. Acc.*, 2001, **105**, 413–421.
11. R. D. Johnson, K. K. Irikura, R. N. Kacker, and R. Kessel, *J. Chem. Theory Comput.*, 2010, **6**, 2822–2828.
12. H. Guo, M. L. Muro-Small, S. Ji, J. Zhao, and F. N. Castellano, *Inorg. Chem.*, 2010, **49**, 6802–6804.